M2LW-21OR0402036

Light Water Reactor Sustainability Program

Evaluation of Stress Corrosion Cracking Behavior of Ni-base Alloys in PWR Primary Water Containing KOH vs. LiOH

September 2021

U.S. Department of Energy

Office of Nuclear Energy

M2LW-21OR0402036

Evaluation of Stress Corrosion Cracking Behavior of Ni-Base Alloys in PWR Primary Water Containing KOH vs. LiOH

Ziqing Zhai
Mychailo B. Toloczko
Ferdinan C. Colon
Ryan A. Bouffioux

September 2021

Prepared for the
U.S. Department of Energy
Office of Nuclear Energy

ABSTRACT

The U.S. nuclear industry is considering replacing lithium hydroxide (LiOH) with potassium hydroxide (KOH) for pH control in pressurized water reactor (PWR) primary water for economic reasons. Among the many aspects of reactor operation that need to be assessed before switching to KOH, it is necessary to evaluate the stress corrosion cracking (SCC) response of Ni-base alloys in a KOH environment to ensure that SCC susceptibility is not increased by KOH water chemistry. In collaboration with an ongoing Electric Power Research Institute (EPRI) -led KOH qualification program, this project is performing SCC evaluations on selected materials in both LiOH and KOH-containing PWR primary water chemistries. This report documents the research progress accomplished in FY21 on this topic with a testing focus on two high-strength Ni-base alloys - Alloy X-750 and Alloy 718. SCC growth behavior is being evaluated using in situ measurement of crack length in PWR primary water chemistry specified by EPRI. KOH and LiOH concentrations were selected to achieve the same pH. The chemistries were changed on-the-fly, allowing uninterrupted, direct comparison of SCC growth rates of KOH vs. LiOH. In addition, SCC initiation behavior of Alloy X-750 was assessed in KOH and LiOH water chemistries. For FY21, comparisons have only been obtained on Alloy X-750, and thus far, no obvious difference has been observed in SCC initiation and growth behavior between the KOH and corresponding reference LiOH water chemistries.

ACKNOWLEDGEMENTS

The authors gratefully acknowledge the financial support from the Office of Nuclear Energy, U.S. Department of Energy, through the Light Water Reactor Sustainability Program. In addition, support is recognized from EPRI for technical guidance on material selection and determination of test methods and the U.S. Nuclear Regulatory Commission for providing test systems for the SCC growth rate testing performed in this study. Dr. John Jackson and Mr. Michael Heighes from Idaho National Laboratory are acknowledged for preparing the Alloy X-750 material used for this study. The authors would also like to acknowledge Dr. Peter Andresen (formerly with GE Global Research Center and currently with Andresen Consulting) for helpful discussions on testing ideas. Key technical assistance from Anthony Guzman, Michael Blazon, and Javier Gutierrez at Pacific Northwest National Laboratory is acknowledged for materials preparation activities.

CONTENTS

FIGURES

TABLES

ACRONYMS

AMS	Aerospace Material Specifications
ASTM	American Society for Testing and Materials
BOC	Beginning-of-cycle
BSE	Backscattered electron
BWR	Boiling water reactor
CMTR	Certified materials test report
CT	Compact tension
DCPD	Direct current potential drop
EDS	Energy-dispersive X-ray spectroscopy
EOC	End-of-cycle
EPRI	Electric Power Research Institute
GEGRC	General Electric Global Research Center
IG	Intergranular
INL	Idaho National Laboratory
KOH	Potassium hydroxide
LiOH	Lithium hydroxide
LWR	Light water reactor
NRC	Nuclear Regulatory Commission
PH	Precipitation-hardened
PNNL	Pacific Northwest National Laboratory
PW	Primary water
PWR	Pressurized water reactor
SAE	Society of Automotive Engineers
SCC	Stress corrosion cracking
SCCGR	Stress corrosion crack growth rate
SE	Secondary electron
SEM	Scanning electron microscopy
TG	Transgranular
UHP	Ultra-high purity
VVER	Voda Voda Energo Reactor (Russian type PWR)
YS	Yield stress

Evaluation of Stress Corrosion Cracking Behavior of Ni-Base Alloys in PWR Primary Water Containing KOH vs. LiOH

1. PROJECT BACKGROUND

1.1 Objective

The LWRS task at Pacific Northwest National Laboratory (PNNL) is primarily directed at investigating the long-term stress corrosion cracking (SCC) behavior of light water reactor (LWR) component materials. The objective is to enable better lifetime performance predictions, safety assessments, and risk management during the extended operation of the nation's existing LWR fleet. The research scope is defined with regulatory and industry needs and is linked to state-of-the-art laboratory testing and microscopic characterizations.

1.2 Background of Current Study

"Western" pressurized water reactors (PWRs), i.e., those based on Westinghouse, Babcock & Wilcox, or Combustion Engineering designs and their licensed derivatives, use isotopically specific Li-7 (i.e., ≥99.94% ^{7}Li as ^{7}LiOH) for primary system pH control to reduce general corrosion and manage crud solubility, transfer, and deposition. Naturally-occurring lithium cannot be used because its ^{6}Li content would generate an untenable increase in the production of tritium, a significant radioactive effluent and waste concern. Due to recent difficulties encountered in procuring the isotopically-specific Li-7 that should be used to prevent tritium generation in PWRs, there is commercial interest in investigating an alternative chemical for pH control [1, 2]. Naturally occurring potassium hydroxide (KOH) has been used for this purpose in VVER (Water-Water Energetic Reactor) reactors for more than 40 years, leading to a proposal to investigate it as an alternative to LiOH to maintain pH control. However, KOH has not been qualified for use in the current "Western" PWR fleet. A key concern regarding this application is the potential effect of KOH on the structural materials employed in the reactor internals. While VVERs have not experienced unusual problems with SCC, they use few Ni-base alloys, whereas "Western" PWRs make greater use of Ni-base alloys and their welds in the primary system and pressure boundary components. Therefore, among the many aspects of reactor operation that need to be assessed before switching to KOH, it is necessary to evaluate the SCC response of Ni-base alloys in a KOH environment to ensure that SCC susceptibility is not increased by KOH water chemistry. In support of a qualification program on KOH for PWR primary coolant pH control developed and implemented by the Electric Power Research Institute (EPRI) [2], PNNL has begun SCC testing on selected Ni-base alloys in 2021 to evaluate the effect of KOH vs. LiOH on SCC initiation and growth behavior of these materials. The testing materials and water chemistry conditions were selected based on discussions with EPRI to complement the testing carried out on their own [1, 3]. The test results will help determine if a plant demonstration of the use of KOH is acceptable from a materials-related damage perspective.

1.3 Focus of Current Report

This report documents the first-year research activities on SCC crack initiation and growth behavior of Ni-base Alloy X-750 and Alloy 718 in LiOH and KOH containing PWR primary water. The testing materials and the evaluated water chemistry conditions were selected based on discussions with EPRI, who is organizing a qualification program to assist the US PWR utilities in a potential transition to KOH. SCC initiation tests were performed in two separate test systems in either LiOH- or KOH-containing

beginning-of-cycle (BOC) water chemistry. At the same time, other environmental conditions were kept the same. SCC growth behavior is being evaluated on compact tension (CT) specimens with on-the-fly changes between LiOH- and KOH-containing BOC and end-of-cycle (EOC) water chemistries. The direct current potential drop (DCPD) technique is used for in-situ monitoring of crack extension, allowing direct comparisons on the effect of KOH vs. LiOH on SCC initiation and crack growth behavior of the tested materials. To date, no significant effect of KOH vs. LiOH was observed during the ongoing evaluations.

2. EXPERIMENTAL METHODS

Both SCC initiation testing and SCC growth rate testing are being utilized to evaluate the effect of KOH vs. LiOH on Ni-base alloy SCC in PWR primary water (PW). Since Alloy 718 has the reputation of being very resistant to PWSCC initiation but relatively susceptible to propagation once an intergranular (IG) crack is initiated [4], SCC initiation testing was only performed on Alloy X-750. At the same time, SCC growth behavior is being investigated for both Alloy X-750 and Alloy 718. This chapter will describe these two testing methods in detail to facilitate result interpretation presented later in Chapters 4 and 5. A special focus will be given to explain how on-the-fly water chemistry change between KOH and LiOH was performed during SCC growth rate testing, which enables direct comparison of the effect of KOH vs. LiOH without disrupting the test. In addition, microscopy characterization techniques used in this study will also be introduced.

2.1 SCC Initiation Test Systems and Testing Approach

The SCC initiation testing is performed in state-of-the-art multi-specimen autoclave systems equipped with an active loading unit, a flow loop for water chemistry control, and in-situ DCPDs monitoring for crack initiation.

30.4 mm (1.2-inch) tall uniaxial tensile specimens are used for the tests (Figure 1). All specimens have an identical gauge length of 4 mm. The load on the loading string(s) is applied by a precision servo-electric load control system using a target load of 4670 N (~1050 lbs). Different stress levels can be achieved by varying the gauge diameter in the specimens loaded in the same string, allowing multiple specimens to be tested at their yield stress (YS) or any other target stress. For most specimens, a 1 μm surface finish was prepared to facilitate the examination of precursor damage and cracks on the surface.

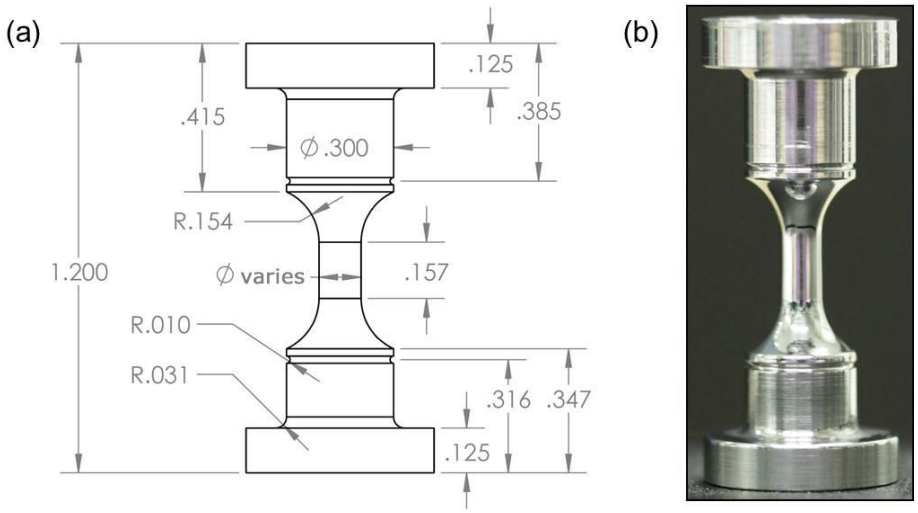

Figure 1. PNNL initiation specimen design. Gauge diameter is selected based on material strength and can be varied from 2.75-4.5 mm (0.11-0.18 inches) and the gauge length is 4.0 mm (0.157 inches). Overall height is 30.5 mm (1.2 inches). Illustrated dimensions are in inch units.

Figure 2 shows the load train and DCPD instrumentation for the typical SCC initiation specimen set up at PNNL. Currently, two medium-size SCC initiation systems and one large SCC initiation system are being used under the scope of LWRS. The two medium-size systems can test up to 6 fully instrumented

specimens, and the large SCC initiation system allows 36 specimens to be tested simultaneously with up to 24 specimens instrumented. The KOH vs. LiOH SCC initiation testing on Alloy X-750 utilized the two medium-size LWRS test systems for "batch testing." One system was filled with LiOH-based water chemistry, and in the other medium-size system, KOH was used at a concentration that provides the same pH as LiOH (neutral pH at 310°C). Six specimens were tested in each water chemistry. To acquire results within a practical timeframe, the tests were performed with accelerant factors in temperature and dissolved hydrogen level. A higher temperature (360°C) than in service (325°C) was used for these tests. In addition, a dissolved hydrogen concentration was selected that corresponds to an electrochemical corrosion potential at the Ni/NiO stability line, where the SCC initiation susceptibility is believed to be the highest for Ni-base alloys.

A reversing DCPD technique developed by General Electric [5] was adapted for online monitoring of SCC initiation behavior based on original work by KAPL [6]. Details of the PNNL approach were provided in previous publications [7, 8]. In the SCC initiation testing of Alloy X-750 to evaluate the KOH vs. LiOH effect, all specimens were tested at or just slightly above their yield stress under constant load. The full load was applied to the specimens within 1–2 days of reaching the test temperature. At the start of a test, the target load (the load at ~0.2% plastic strain) was achieved over a period of 1–2 hours at a constant strain rate of $\sim 1 \times 10^{-5}$ s^{-1}. This displacement rate allows monitoring the strain evolution by DCPD with a sufficiently low noise level. As shown for example in Figure 3, some specimens may yield slightly earlier than the others in a multi-specimen load train system due to intrinsic differences in yield strength and/or gauge diameter. In such a case, small amounts of plastic strain up to ~1.5% are allowed in these specimens to achieve a minimum of 0.15% plastic strain in the others. The specimens are then held at an actively controlled constant load until DCPD detects crack initiation. All relevant environmental parameters and DCPD data are monitored and periodically written to a file. In case that a test is interrupted for specimen examinations or to remove an initiated specimen, the remaining specimens will be taken back to their original load after the test restarts, again following the same steps described above where stress versus strain response is monitored. Figure 4 shows the evolution of both the non-referenced and the referenced strains throughout the exposure of an Alloy 600 specimen. As mentioned above, by subtracting the reference voltage from the gauge voltage, the contributions of resistivity drift and creep are largely eliminated in the referenced strain response. While cracking and some amount of creep contribute to the observed DCPD response simultaneously, the crack initiation time is determined when an apparent increase occurs in the strain rate above the noise level. This is thought to be the onset of fast cracking.

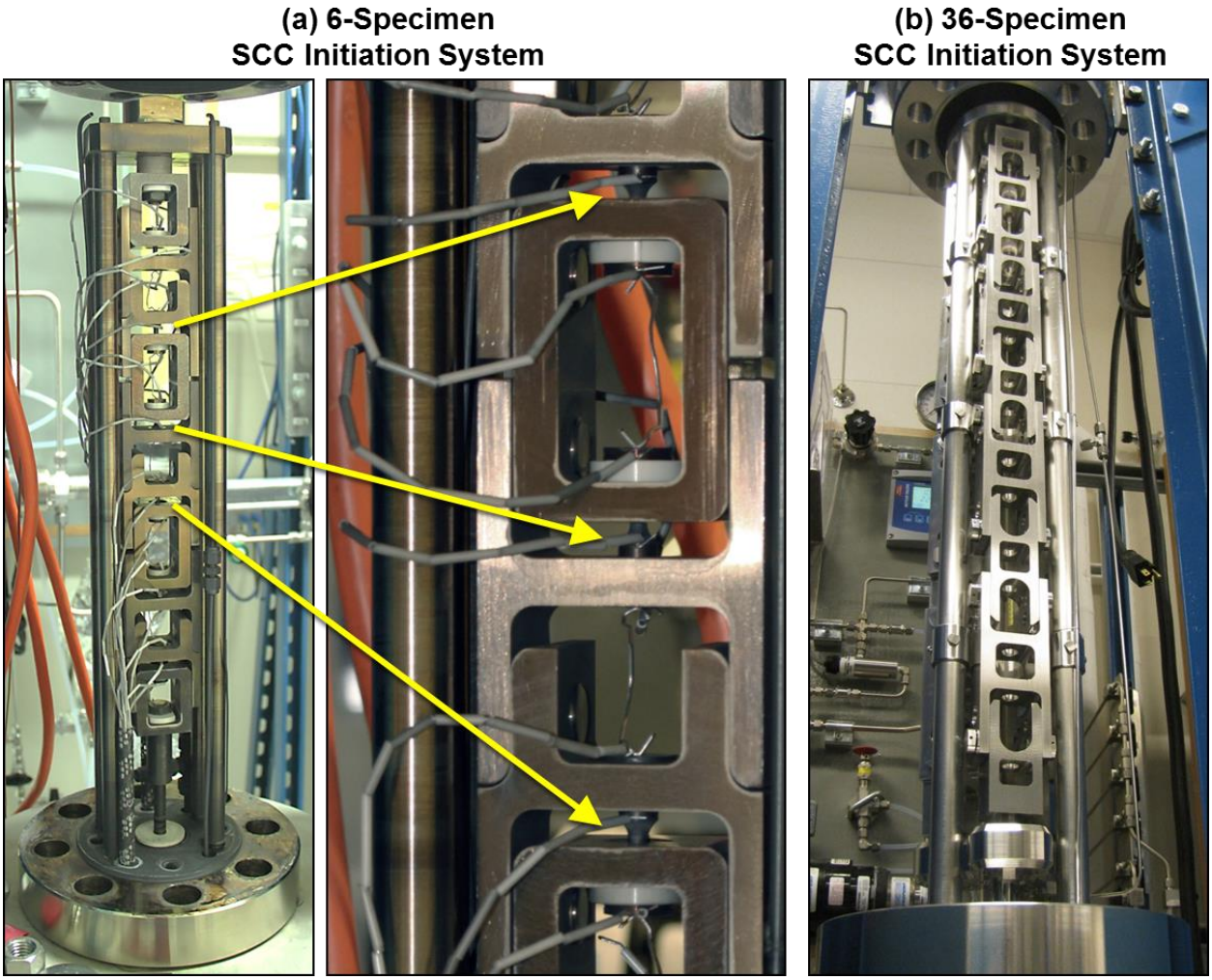

Figure 2. Crack initiation test system load train at PNNL in the (a) medium-size SCC initiation test system with a capacity of testing up to 6 fully instrumented specimens and the (b) large-size SCC initiation test system with a capacity of testing up to 24 instrumented specimens and up to 36 specimens in total.

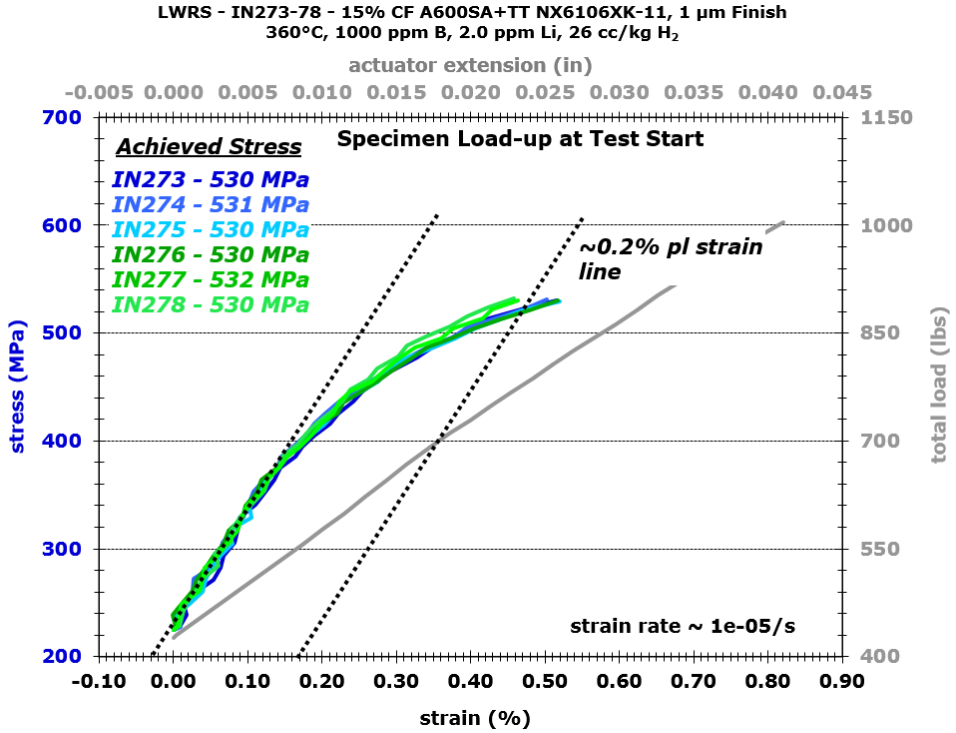

Figure 3. Example of stress versus strain plot during the initial loading of tensile specimens for SCC initiation testing. The displacement in the actuator and the total load is plotted in the secondary x (upper) and y (right) axis, respectively.

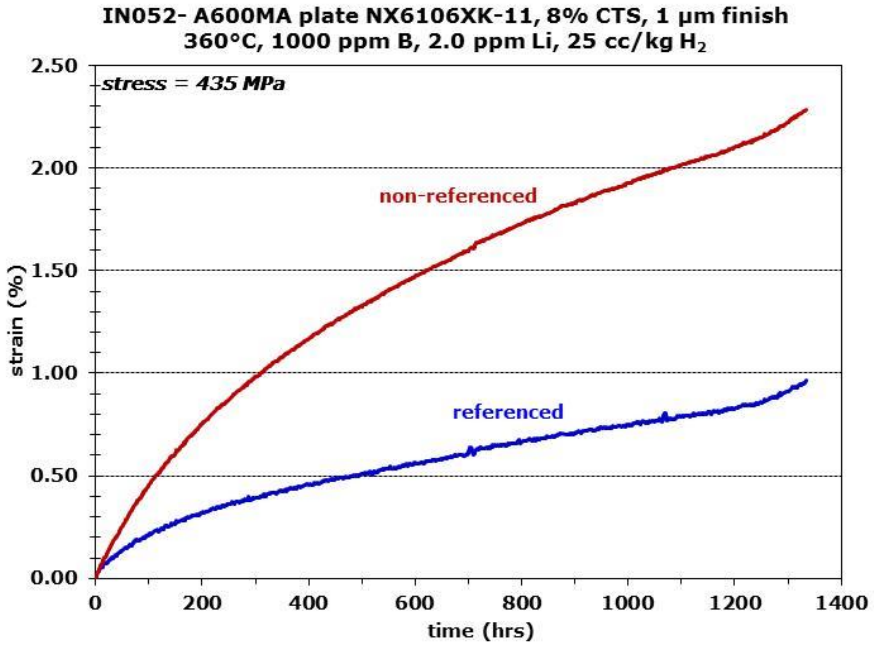

Figure 4. Non-referenced and referenced DCPD strain response for IN052, an 8% CW specimen from Alloy 600MA plate heat NX6106XK-11.

2.2 SCC Crack Growth Test Systems and Testing Approach

2.2.1 Overview of SCC Crack Growth Test Systems

Although the LWRS SCC initiation test systems can be converted to perform stress corrosion crack growth rate (SCCGR) evaluations, they are fully occupied in FY21 by SCC initiation testing of cold-worked Alloy 690 and Alloy X-750. As a result, two U.S. Nuclear Regulatory Commission (NRC) owned SCCGR test systems were borrowed under an agreement to investigate the effect of KOH vs. LiOH on the SCC growth behavior of Alloy X-750 and Alloy 718.

The NRC SCCGR test systems at PNNL were designed and constructed to measure crack length under well-defined material and environmental conditions and ensure that the growth rate response is reproducible and characteristic of the test conditions. An example of the SCCGR test system is shown in Figure 5. Detailed information on the development of these test systems can be found elsewhere [9]. However, two key features of these test systems are reviewed here because they are important to the KOH vs. LiOH evaluations.

Firstly, crack length is measured in-situ. This has high value because it allows for evaluating SCCGR response before and after "on-the-fly" changes in environmental conditions. For SCCGR testing, it is the best means to ensure that a measurement is not affected by extraneous parameters associated with alternative approaches such as stopping a test to change water chemistry. On-the-fly evaluations are also time and cost efficient.

Secondly, control of ion species in the test system recirculating water loop is attained using a mixed bed demineralizer. For testing in simulated standard PWR primary water, a controlled amount of boric acid and lithium hydroxide are introduced to the demineralizer. An amount is selected such that stable B and Li values are attained in the test system water, i.e., the demineralizer neither absorbs nor releases B and Li as the water passes through it when no other ions are present. The relevance to the KOH evaluation effort is that this approach to PWR primary water chemistry simulation requires preparing a dedicated demineralizer for each water chemistry to be investigated. It also requires a carefully planned procedure for swapping out water on-the-fly. This approach will be discussed in detail in the next section.

Figure 5. Typical SCCGR test system used at PNNL.

2.2.2 General SCC Crack Growth Testing Approach

Although the PNNL SCCGR test systems have been designed for use with both 1T and 0.5T CT specimens, the primary specimen geometry used in this project is the 0.5T CT with side grooves. The details of the specimen geometry are shown in Figure 6. Prior to loading a specimen in the autoclave, the sample thickness, notch depth, and width values are all measured and recorded into the data record for the test. Using the sample dimensions and the yield strength (YS) of the specimen at the test temperature, following American Society for Testing and Materials (ASTM) Standard E-1681, an upper limit on the value of the stress intensity (K) is calculated using the formula:

$$K = \sigma_{ys}\sqrt{D/1.27} \quad (1)$$

where σ_{ys} is the YS at the test temperature and D is the smallest of the specimen thickness, the remaining uncracked specimen width, and the crack length. In the case of materials with large amounts of work hardening (where the ratio of ultimate tensile strength to yield strength is greater than 1.3), such as annealed 300-series stainless steels and Ni-base alloys, the average of the yield and ultimate stress is used in place of the YS following ASTM guidelines. This value is not considered a strict limit but rather provides a reference point for what may be considered a high-stress intensity for a given material.

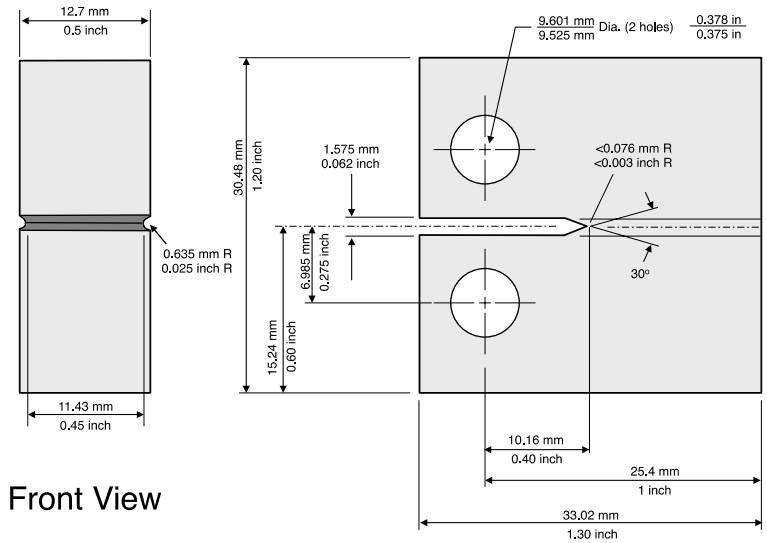

Figure 6. Schematic drawing of a 0.5T CT specimen. Oversized loading holes (~9.5 mm diameter) are used to accommodate ceramic inserts that provide electrical isolation between the CT specimen and clevises. The dimensions for 1T CT specimens are approximately double.

Crack growth tests are usually performed with two specimens load in series into a test system, allowing a greater range of material conditions to be examined in a shorter period of time, or to assess test reproducibility by using two samples from the same material condition. After the sample dimensions are measured, and spot-weld locations are marked on the sample, it is cleaned and inserted into a test system. Precracking of a sample is done in situ at the test temperature when a single specimen is being tested. Initial precracking of two or more specimens mounted in series is not possible in situ because the length of time needed to nucleate a precrack is not consistent. Consequently, precracking two specimens in series would likely lead to specimens having different precrack lengths. The differing precrack lengths would make it impossible to maintain and control the K level in both specimens during and after precracking. Thus, the approach for testing at PNNL is to nucleate a crack individually on each of the two specimens under fatigue in air, followed by continued precracking of the two samples loaded together in situ. Crack transitioning steps are carefully selected to grow the precrack in high-temperature water using the following stages: (1) fatigue, (2) corrosion fatigue, and (3) SCC. Typically, this means producing initial precracks of ~1 mm in air followed by an additional ~1 mm by cycling in situ before transitioning to slow cyclic loading plus hold times to promote SCC. An Instron servohydraulic test frame is used to precrack CT specimens in air, and the same DCPD electronics and system control software used for the crack growth systems is also used for the Instron test frame.

The first step in precracking is to cycle the sample at a relatively high frequency (2–10 Hz) with a large load ratio (R) and K_{max} less than or equals to the K level chosen for constant K. As the crack begins to grow from the notch, R is increased and frequency is reduced while the K_{max} value is increased. By precracking in this way, each precrack segment can grow beyond the plastic zone created by the previous segment. For all samples, cyclic loading steps at frequencies of 0.1 Hz down to 0.001 Hz are performed in high-temperature water. The final phase involves crack transitioning by very slow cycling with a hold time ranging from 1 h to 24 h. This grows the crack beyond the precracking plastic zone and allows the crack to transition from transgranular (TG) fatigue to the crack growth morphology that normally occurs under constant K conditions. Depending on the material susceptibility, this may be either TG or intergranular (IG) cracking. For materials such as Alloy X-750 and Alloy 718 that readily undergo intergranular SCC growth in LWR environments, obtaining a steady SCC growth rate after transitioning to constant K can easily be accomplished by following a standard procedure, which will be presented later in Chapters 4 and 5.

2.2.3 Uncertainties in Crack Growth Data Measurements

While the noise resolution of the PNNL DCPD test method is more than ±3 μm and allows for establishing trends in the CGR down to ~$5x10^{-10}$ mm/s, the accuracy of these rates depends on some factors that cannot be fully assessed. For example, crack front irregularity can affect the DCPD-measured growth rate. Still, there is no way to document the variation in the shape of the crack front as the crack grew, and therefore, this effect cannot be accurately included in post-test crack length corrections. Another issue is that it is often not possible to uniquely identify each phase of a test on a crack surface after the test has ended. As a result, the post-test correction is typically based on the entire in situ portion of the test. An additional complication is the effect of ligament or contact formation on constant K crack growth. Even though attempts are made during the test to assess these effects, there are no post-test means of assessing exactly how well this method works. Crack growth testing experience and interactions with the international expert community have produced many insights into issues, but many uncertainties cannot be effectively quantified. Based on our experience, state-of-the-art testing methods, and data analysis approach, we believe overall uncertainties for crack growth-rate measurements are on the order of ±50% for SCC-susceptible materials with steady growth response. Uncertainty in reported stress intensity for a relatively straight final crack front is ≤10% after correcting for observed crack length. Still, for a highly uneven final crack, the local variability is not easily quantified and may be substantial.

2.2.4 Water Chemistry Control for the KOH vs. LiOH Study

This study aims to produce quantitative SCCGR data through in-situ measurement of crack length in KOH-based water chemistries and in corresponding reference LiOH-based water chemistries that will serve as the point of comparison. The water chemistries to be evaluated in the SCC growth rate testing were determined by EPRI with details listed in Table 1. The effects of KOH relative to LiOH will be evaluated at beginning of cycle (BOC) water chemistry and end of cycle (EOC) water chemistry. A mid-cycle water chemistry will also be evaluated. This mid-cycle B/K chemistry is being evaluated because during reactor operation, B-10 decays by thermal neutron absorption to produce Li-7: $^{10}B(n,\alpha)^{7}Li$ [1]. LiOH and KOH concentrations were selected to provide neutral pH at 310°C. pH at the 360°C test temperature is slightly basic. For these particular bases, this occurs at molar-equivalent concentrations.

Table 1. Nominal PWR primary water chemistries identified by EPRI for the KOH vs. LiOH study.

Environment	ppm B, ppm Li, or ppm K	pH(310°C)	pH(360°C)
BOC	1500 B / 2.2 Li	7.0	8.39
	1500 B/ 12.4 K		
EOC	10 B / 0.23 Li	7.0	8.26
	10 B / 1.30 K		
Mid-cycle	1000 B / 3.3 K + 1.0 Li	7.0	8.36

The key to the test is to make on-the-fly changes between Li- and K-containing water chemistries with no change in any other conditions. By following this methodology, direct comparison of SCCGR of KOH vs. LiOH is obtained with no other changes to the test. To achieve this, the desired test system water and corresponding demineralizer filters were prepared beforehand. Mixed bed demineralizer filters were equilibrated to the designated chemistry at room temperature by circulating deaerated water through a loop with the demineralizer and adding the corresponding chemicals until the desired B and Li or K values are attained and are stable.

To gain experience and ensure that the on-the-fly water chemistry changes would be successfully implemented during testing, a water chemistry change trial from 1500 ppm B/2.2 ppm Li to 1500 ppm B/12.4 ppm K and then to 10 ppm B/0.23 ppm Li was performed before the start of the actual tests. All the other environmental conditions (e.g., temperature, dissolved hydrogen, etc.) were set to the same

target values used in the test. A simplified water board set up in preparation for these changes is illustrated in Figure 7. The on-the-fly changes were accomplished by draining 95 volume% of the old solution inside the water column and then switching the inlet flow to draw water from the prepared new deaerated solution in a five-gallon container. This refills the water column and pushes the new solution through the autoclave and the water board. In addition, the solution being purged from the autoclave was decanted into a disposal container during all autoclave volume exchanges using the outlet before reaching the demineralizer filter (Figure 7). This process is repeated approximately for five–six autoclave volume exchanges. The first three exchanges take place with the demineralizer valved out from the water chemistry control board. After the third volume exchange, a demineralizer configured for the new target water chemistry is valved in. Table 2 summarizes the evolution of monitored environmental parameters during the entire process of an on-the-fly water chemistry change trial run from 1500 ppm B/2.2 ppm Li to 1500 ppm B/12.4 ppm K. The changeover usually took ~5 hours to complete, but 24 hours was given for the system to equilibrate. Whether the final concentration of the solution is on par with the target can be determined by acquiring a water sample after the equilibration is reached.

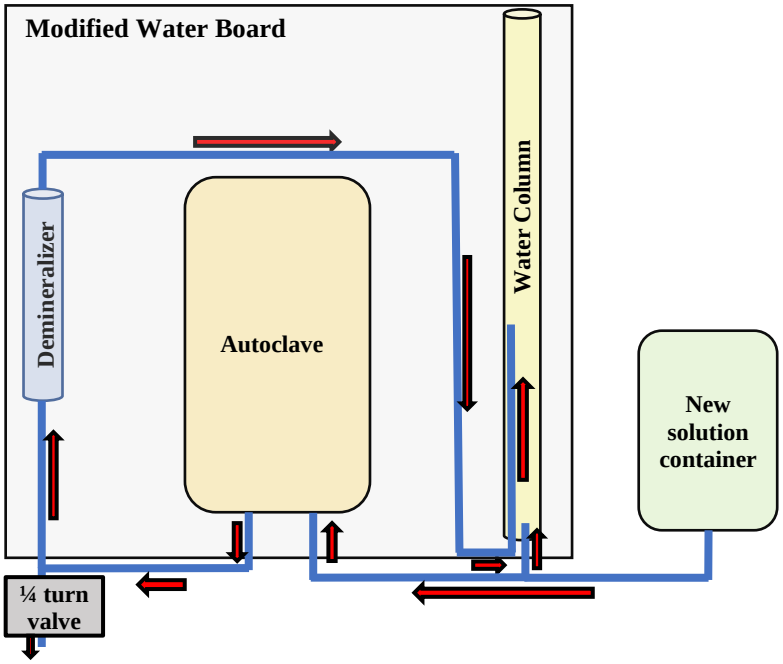

Figure 7. Simplified schematic of the modified water board setup for on-the-fly chemistry changes used in the SCCGR test system. The red arrows indicate the direction of the water flow.

Table 2. Environmental parameter tracking at each autoclave volume exchange during the trial on-the-fly water chemistry changeover from 1500 ppm B/2.2 ppm Li to 1500 ppm B/12.4 ppm K.

Vol. change #	Resistivity (Kohm-cm)	Conductivity (µS/cm)	pH	Temp (°C)	B content (ppm)	Li content (ppm)	K content (ppm)
0	47.32	21.13	6.15	23.45	1512	2.19	0
1	38.78	25.79	N/A	24.89	N/A	N/A	N/A
2	36.62	27.31	N/A	24.97	N/A	N/A	N/A
3	35.17	28.43	N/A	25.00	N/A	N/A	N/A
4	33.90	29.49	N/A	24.94	N/A	N/A	N/A
5	29.83	33.52	6.09	23.55	1637	~ 0	12.97
6	30.21	33.10	6.18	23.49	1501	~ 0	12.77

2.3 Microstructural Characterizations

2.3.1 Pre-Test Microstructure Examinations

Both optical microscopy and scanning electron microscopy (SEM) were utilized to document the microstructure of Alloy X-750 and Alloy 718. Three ~10×10 mm pieces were sampled to allow documenting the microstructure in the "A", "B", and "C" observation directions of the Alloy X-750 and Alloy 718 materials following the designation specified in Figure 8.

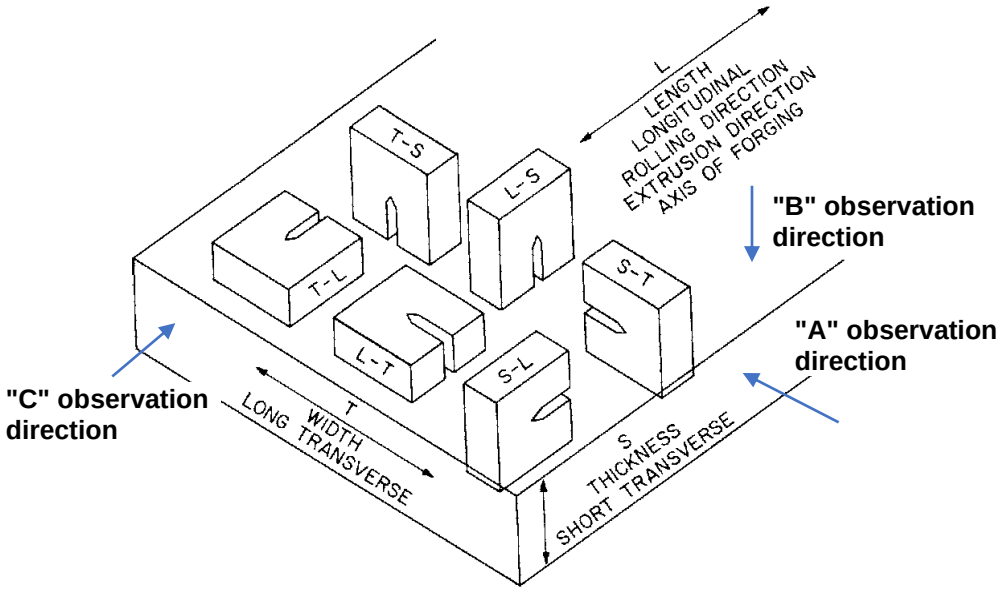

Figure 8. Definitions of the S-L, T-L, and S-T crack growth planes relative to plate fabrication conditions. The first letter indicates the cracking plane, and the second letter indicates the crack growth direction in that plane. "A", "B", and "C" observation directions are noted.

The metallographic examinations of the Alloy X-750 and Alloy 718 materials were performed using an Olympus BX51M optical microscope with DP74 camera to examine grain size, precipitate distribution, and the presence of banding. The samples were polished to a colloidal silica finish and then dip-etched for ~1 min in Kalling's #2 etchant (100 mL ethanol, 100 ml HCl, 5 g $CuCl_2$) to reveal grain boundaries and precipitates. Large mappings of an area of ~6×4 mm were acquired on all three planes under darkfield conditions at a resolution of 0.59 µm/px for each optical micrograph. Acquisition routines were performed using Olympus Stream v2.2 software for stage control and collage assembly.

High-resolution SEM examinations were performed on all non-etched samples to identify intragranular and IG precipitates and confirm microstructure. This task was performed using a JEOL 7600F scanning electron microscope with most images acquired at a low-kV backscattered electron (BSE) mode. Energy-dispersive X-ray spectroscopy (EDS) was also employed to help identify the type of precipitates found in the materials.

2.3.2 Post-Test Specimen Examinations

For SCC initiation specimens, the post-test examination focuses on documenting the entire gauge surface of all specimens to check if any difference in cracking morphology is present between specimens tested in the KOH- vs. LiOH-containing water chemistries. Again, the JEOL 7600F scanning electron microscope is used for this task. Four fiducial scribe marks (90° to one another) were made at the button ends of each specimen to keep track of the specimen orientation. Each of the four rotations was then

mapped using high-kV BSE montage imaging to reveal IG damage features covered under thin surface oxides. Figure 9 illustrates that the surface of the entire gauge section and part of the fillet region were mapped for each rotation. Oxford Aztec software was used to automate stage movement such that the gauge surface of each rotation could quickly be mapped, enabling montages to be created. The montages from the four rotations were then stitched together manually in Photoshop for crack mapping.

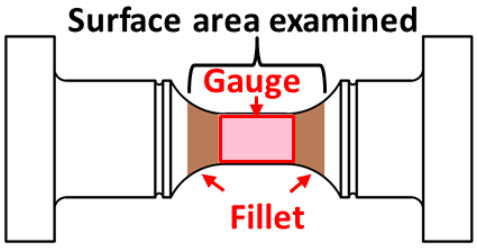

Figure 9. Schematic of the surface area of one rotation mapped in SEM for pre-test examination. The gauge surface mapped in SEM is highlighted in pink, and the surface in the fillet region mapped in SEM is highlighted in taupe.

Following the standard practice at PNNL, the post-test examination plan of tested CT specimens will involve cutting the CT specimens into 1/3 and 2/3-thickness slices in the thickness direction [9]. The 2/3-thickness slice is fatigued open in air for crack surface observations to compare the actual crack extension with the crack length estimated by DCPD and determine if any corrections need to be made. The cut surface of the 1/3-thickness slice will be polished to a colloidal silica finish to provide a cross-section observation of crack morphology. Other characterization high-resolution microscopy techniques, such as transmission electron microscopy or atom probe tomography, may be employed if there is an interest in investigating local chemistry at or near the crack tip. As of this writing, the SCC growth rate testing on Alloy X-750 and Alloy 718 is ongoing, so no post-test examinations have been performed on the CT specimens.

3. TESTING MATERIALS

Based on discussions with EPRI, the first-year SCC testing at PNNL on the effect of KOH vs. LiOH focuses on Alloy X-750 and Alloy 718, both of which are high strength Ni-base alloys. Alloy 600 and its weld metal - Alloy 182 - have already been evaluated by EPRI as part of their qualification program on KOH for PWR primary coolant pH control [3]. Alloys X-750 and 718 are commonly used in LWRs for springs and fasteners, often in situations close to the fuel where irradiation exposure is high. They were often chosen for their high strength, general corrosion resistance, and resistance to irradiation-induced relaxation. The Alloy X-750 material evaluated in this study is a commercial Alloy X-750 heat originally sourced from a utility by EPRI with known susceptibility to SCC. The Alloy 718 material used for this study was fabricated by Special Metals and was purchased in a solution annealed condition. An LWR-relevant thermal treatment was applied in-house. In this chapter, the thermal-mechanical history and microstructure of these testing materials will be provided. The selection of testing orientations for SCC initiation and crack growth specimens will also be presented.

3.1 Alloy X-750

3.1.1 General Information of the Selected Heat

The Alloy X-750 material used for this study was purchased from Southern Co. by EPRI. Originally intended for a boiling water reactor (BWR) core shroud tie rod repair, it was removed from a spare upper support bracket and sent to GEGRC and Idaho National Laboratory (INL) for fracture toughness and SCC evaluation in BWR environments [10, 11]. As part of an EPRI's BWR Vessel and Internals Project, the bracket was dissembled, and one of the arms was sectioned into several parts (Figure 10) for detailed characterizations. The support bracket was machined from a 51.3 mm thick by 1219 mm wide by 2438 mm long plate of Alloy X-750 from Haynes International heat 2750-5-7656. The heat chemistry shown in Table 3 is from the certified materials test report (CMTR). Alloy X-750 is a gamma prime (γ') (Ni_3[Ti,Al]) precipitation strengthened superalloy designed for high-temperature strength, oxidation, and creep resistance, and is used in structural support applications for LWRs. The composition of Alloy X-750 is close to that of Alloy 600 except for higher contents of titanium (Ti), aluminum (Al), and additions of niobium (Nb), which are the primary strengthening elements. High strength is developed by heat treatment after solution annealing that leads to a homogeneous distribution of gamma prime precipitates that are coherent with the austenite matrix. Among the choices of heat treatment available for Alloy X-750, two have been used extensively: a two-step thermal treatment at 885°C and 704°C (AH), or a high-temperature solution annealing at ~1100°C followed by single-step aging at 704°C for 20 hours and air cool (HTH) [12, 13]. The latter optimizes the precipitation of grain boundary carbides that appears to confer maximum resistance to PWSCC provided thermal aging is preceded by at least 40% cold work. The heat treatment condition of the as-supplied plate was not specified. A subsequent full heat treatment was performed by INL and consisted of a solution anneal step at 1107°C for 1 hour, followed by a water quench, and then a γ' precipitation heat treatment of 704°C for 20.25 hours.

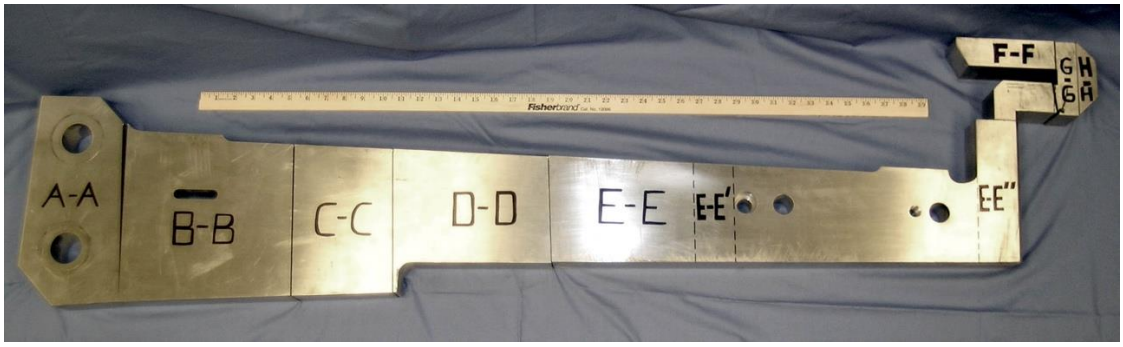

Figure 10. Primary sections cut from one arm of Alloy X-750 stabilizer support bracket [14].

Table 3. Chemical composition (wt. %) taken from the certified material test report of Alloy X-750 heat 2750-5-7656, obtained from billet end compared to the Alloy X-750 specifications. One element name in the document was illegible.

Element	Alloy X-750 Specification	Alloy X-750 Heat 2750-5-7656
C	<0.08	0.04
Cr	14-17	14.99
Fe	5-9	7.80
Mn	<1	0.197
Ni	>70	70.83
Ti	2.25-2.75	2.42
Al	0.4-1	0.77
Co	<1	0.726
P	<0.008	<0.005
Cu	<0.5	0.0151
S	<0.01	0.002
Si	<0.5	0.253
Nb+Ta	0.7-1.2	0.99 (Ta: <0.01)
Unreadable element name in the CMTR		0.976

3.1.2 Characterizations of the Alloy X-750 Material

Macrostructural and microstructural analyses were performed at GEGRC on metallographic samples taken out from all sections the Alloy X-750 stabilizer support bracket (Figure 10) [10]. The description of these features provided here largely follows their reported observations. Overall banding was observed throughout the support bracket in terms of both grain size banding and carbide banding, with a representative example shown in Figure 11. It features alternating regions of significantly different grain sizes produced during fabrication of the plate. It also features prevalent carbide banding. The carbide banding appears as wavy lines of black specks that vary in density. Closer examinations revealed that the small spherical-shaped particles that compose the carbide atmospheres in the bands are secondary MC-type carbides. Larger primary M(C,N) carbonitrides with a blocky morphology are also present in the bands but at lower densities (Figure 12).

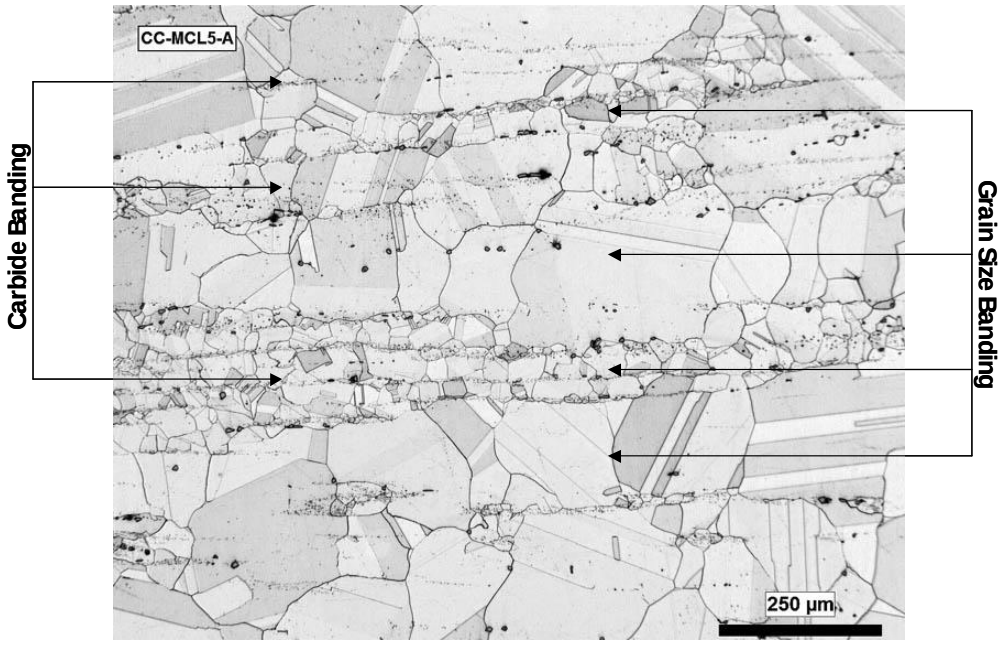

Figure 11. Representative optical micrograph from GE of Alloy X-750 taken from section C-C longitudinal orientation with grain and carbide banding identified [14].

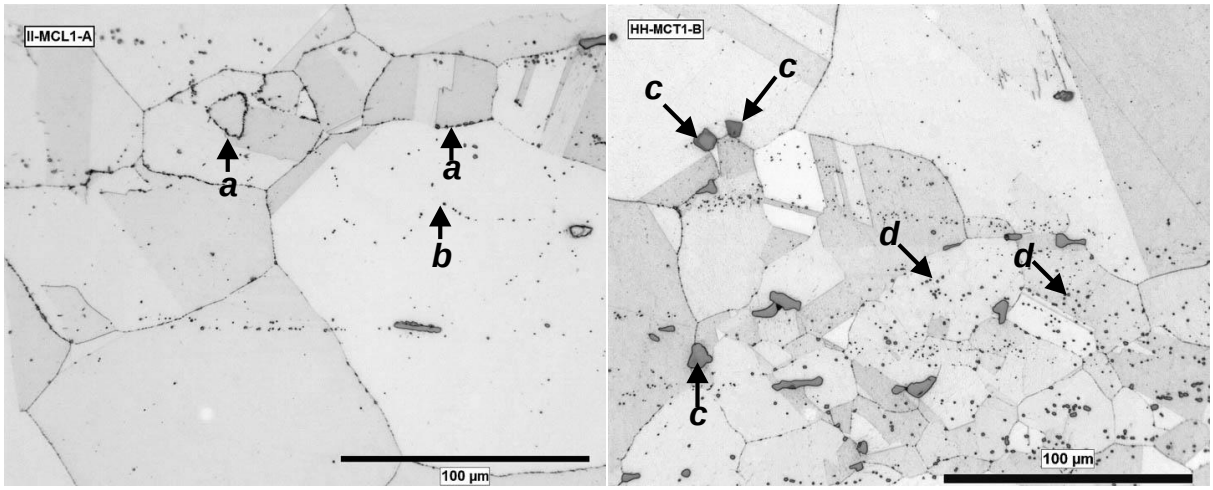

Figure 12. Second phases in GE-acquired optical micrographs of the Alloy X-750. a) grain boundaries decorated with secondary MC-type carbides, b) prior grain boundaries decorated with MC-type carbides, c) primary M(C,N) carbonitrides, d) secondary MC-type carbides [14].

With the facilitation of EPRI, PNNL acquired a leftover block from the C-C section from INL for the current study (Figure 13). Heavier banding has been reported for this section as compared to other sections [14]. To confirm the microstructure, a macroscopic optical analysis of the S, L, and T planes (relative to the plate production direction) in cross section was performed at PNNL on the acquired block following the designation specified in Figure 8. As shown in Figures 14-16, extensive banding microstructures in the S plane can be seen in this material. While often appearing concurrently, carbide banding tends to be more prominent than the bands of finer grains, especially when viewed in the "A" direction. Bands of high-density carbides usually repeat within every 300 µm in the short-transverse direction and exhibit a length of 100s of micrometers to more than 1 mm in the longitudinal direction

regardless of the grain size (Figure 17). In the "B" observation direction, a one-to-one correlation between fine-grain clusters and ultra-dense carbide atmospheres was observed (Figure 15). The "C" observation direction features strata-like carbide banding with the carbide banding appearing more prominent than in the "A" observation direction. In addition, the carbide banding often extends across the entire width (~4 mm) of the field of view (Figure 16). This information helped determine the specimen orientation for SCC testing and is expected to be useful for interpretation the SCC initiation and crack growth behavior observed in the specimens, which will be discussed later.

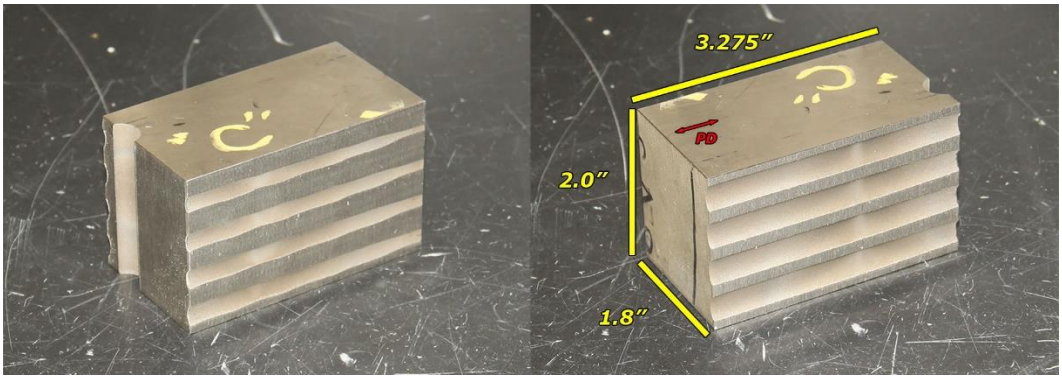

Figure 13. The Alloy X-750 block (heat 2750-5-7656) from Section C-C in Figure 10 received by PNNL for the KOH vs. LiOH primary water chemistry study. The dimensions are specified in inches in the image. “PD” = plate fabrication processing direction.

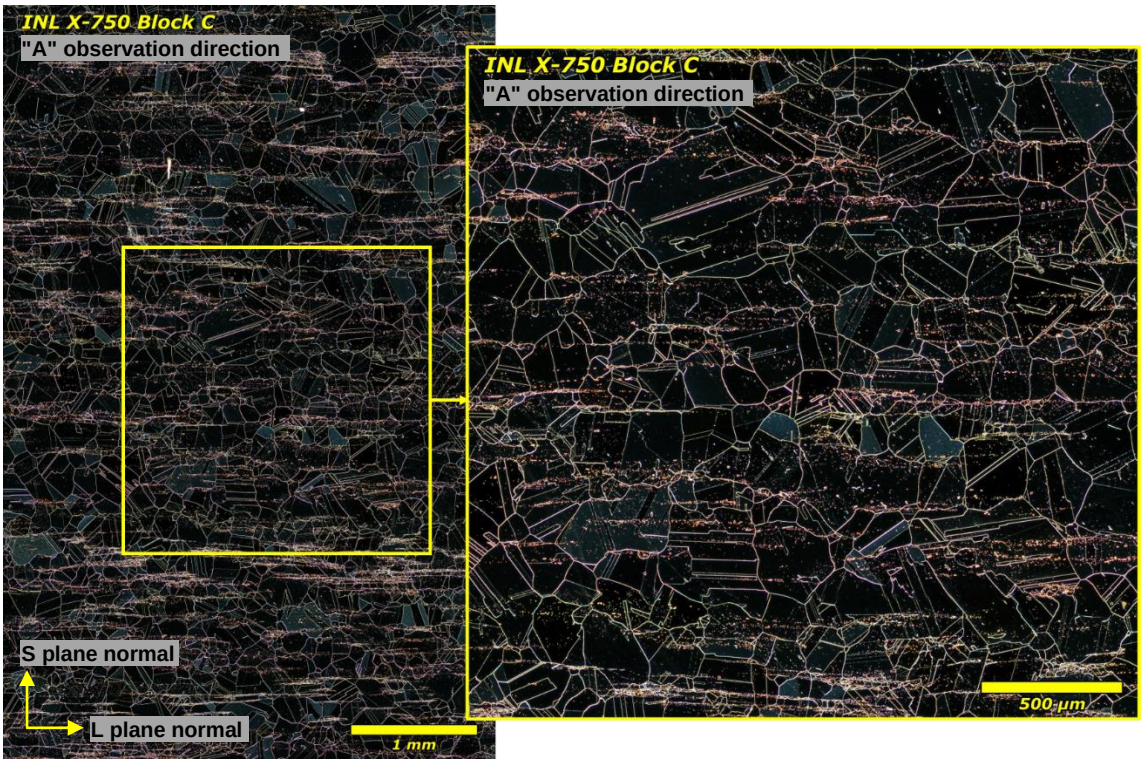

Figure 14. Representative optical micrograph of the banding microstructure revealed in the "A" observation direction of the Alloy X-750 block received from INL (heat 2750-5-7656).

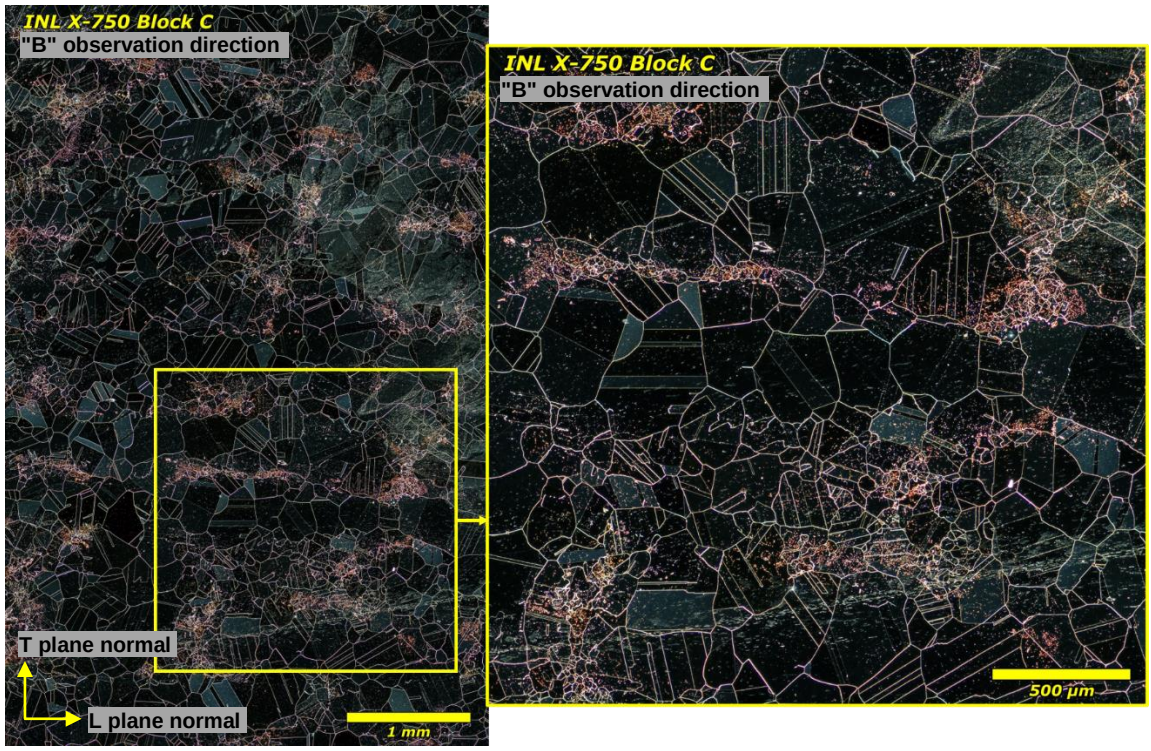

Figure 15. Representative optical micrograph of the banding microstructure revealed in the "B" observation direction of the Alloy X-750 block received from INL (heat 2750-5-7656).

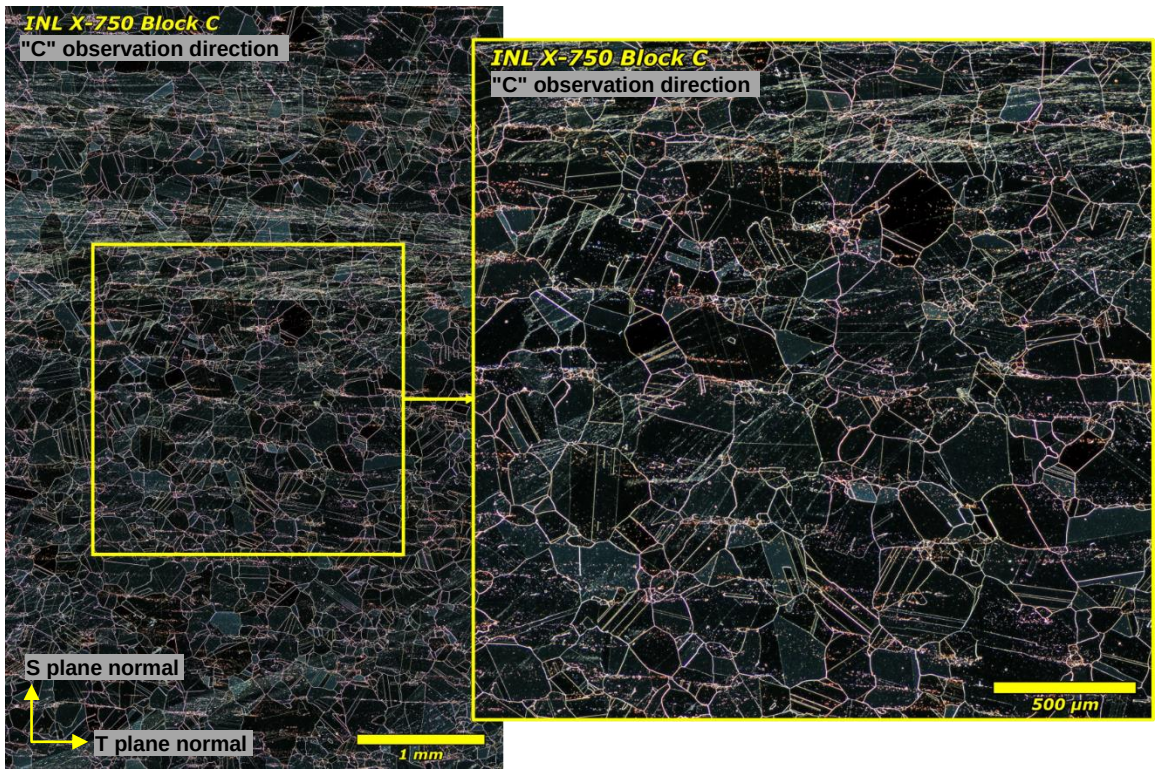

Figure 16. Representative optical micrograph of the banding microstructure revealed in the "C" observation direction of the Alloy X-750 block received from INL (heat 2750-5-7656).

SEM examinations were also performed at PNNL to examine the distribution and type of precipitates in the received Alloy X-750 block, with a focus on IG phases in the fine-grain banding regions as seen in the "A", "B", and "C" observation directions. Samples polished to a colloidal silica finish were used for this purpose. Representative microstructures and grain boundary precipitates are shown in Figures 18 and 19. It is obvious that the high-energy grain boundaries feature a fine disperse of <100 nm precipitates with occasional larger phases of ~500 nm – 1 μm in size. Qualitative SEM-EDS analysis suggested that the fine precipitates are mostly $Cr_{23}C_6$ type carbides and the larger phases are Nb/Ti-rich carbides (Figure 19). High-resolution characterizations performed by GEGRC revealed a duplex γ' size distribution of 5 and 25 nm at grain boundaries, which is consistent with the HTH heat treatment with some variation in the solution annealing process used [14]. Unfortunately, these γ' phases were not resolved at PNNL using the current SEM and EDS imaging conditions. More detailed characterizations using alternative sample preparation techniques such as special etching as GEGRC did, or TEM analysis are planned to better record these fine-size phases.

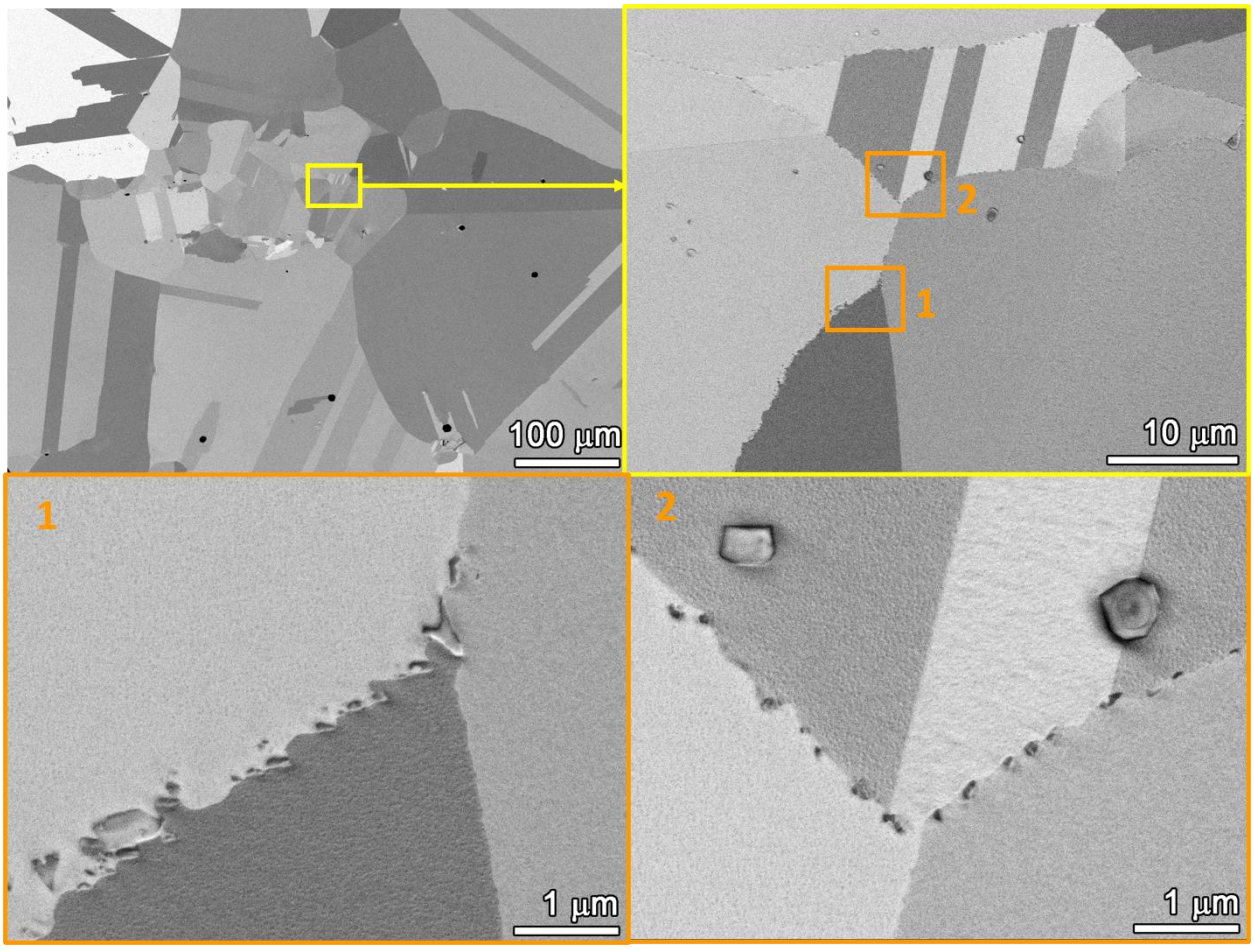

Figure 17. SEM-BSE images showing the grain microstructure and precipitation distribution in the fine grain banding in the "A" observation direction of the Alloy X-750 block received from INL (heat 2750-5-7656).

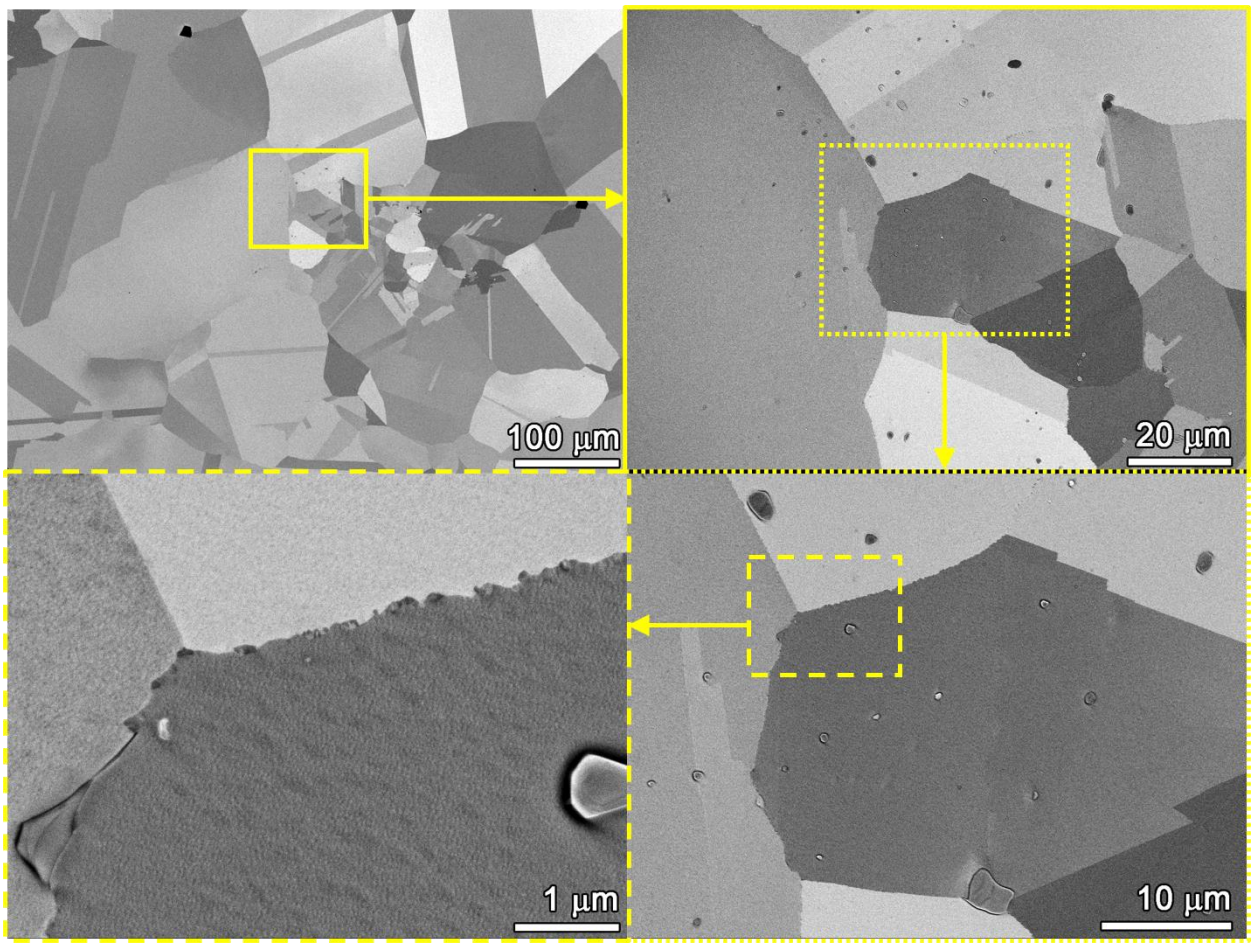

Figure 18. SEM-BSE images showing the grain microstructure and precipitation distribution in the fine grain banding region in the "B" observation direction of the Alloy X-750 block received from INL (heat 2750-5-7656).

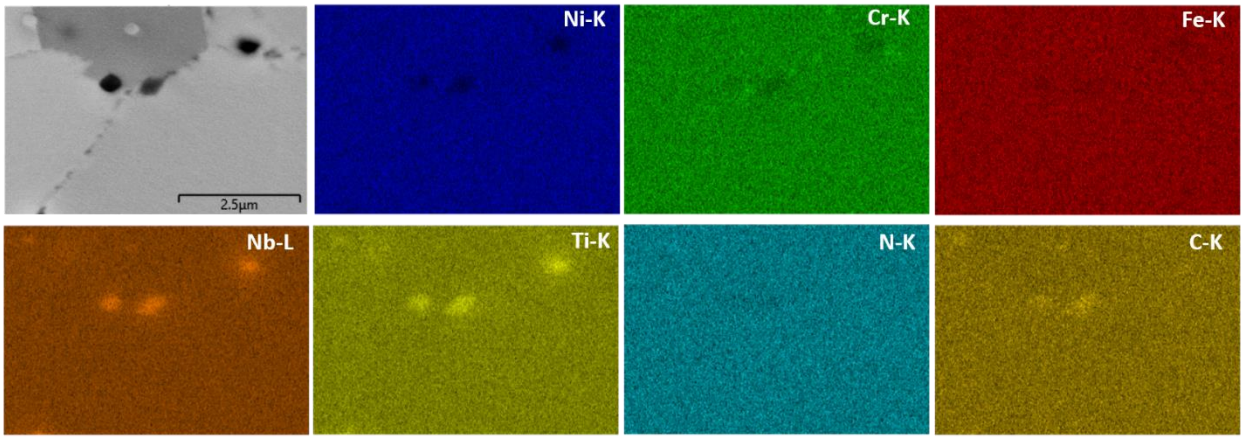

Figure 19. Qualitative SEM-EDS analysis of the chemical composition of the grain boundary precipitates observed in the "A" observation direction of the Alloy X-750 block received from INL (heat 2750-5-7656).

3.2 Alloy 718

3.2.1 General Information

Alloy 718 is an age-hardenable nickel-base alloy containing 17-21% Cr and a higher niobium (Nb) content than Alloy X-750. It can be heat treated to very high strength due to precipitation of a fine distribution of nanometer size γ', Ni_3(Al,Ti), and γ", Ni_3(Nb). Alloy 718 has found increasing use in LWRs for springs and bolts in fuel elements because of its significant strength and resistance to corrosion and thermal/irradiation-induced relaxation. Service experience has generally been good, but recently there have been instances of cracking and deleterious effects, leading to early assembly discharge and, possibly, fuel failures [15]. Early LWR applications of Alloy 718 usually adapted heat treatments intended for aircraft engine and gas turbine applications. While these heat treatments produce grain boundary precipitates that were very beneficial for minimizing high-temperature creep, the precipitates themselves are not necessarily beneficial for SCC resistance in LWR environments. This is often correlated with the presence of the δ phase, Ni_3Nb. δ phase is a thermodynamically more stable form of the γ" strengthening phase. Its formation results in γ" denuded zones on either side of grain boundaries that may in principle allow localized strain concentration [16, 17]. However, others have not observed a major effect of δ phase on product performance, and indeed note that it is a necessary feature to avoid excessive grain growth during solution annealing prior to thermal aging [4]. Subsequent commercial heat treatments developed for Alloy 718 resulted in high SCC initiation resistance, particularly in PWR environments. However, test results from these commercial heats show that crack propagation rates could be quite high depending upon the type of heat treatment [15].

For this study, PNNL purchased a L14" × W4" × T2" block from an Inconel Alloy 718 plate heat HT6097EK11 manufactured by Special Metals. It has typical Alloy 718 composition in conformance with Alloy 718 specifications as listed in Table 4. The material was solution annealed and certified by Special Metals to Society of Automotive Engineers (SAE) Aerospace Material Specifications (AMS) 5596 [18]. A conventional two-step precipitation hardening heat treatment (age at 718°C for 8 hours, cool to 621°C at 55 °C/h, age for 8 hours, and air cool to room temperature) compliant with SAE AMS5663 [19] was applied to the block at PNNL. This heat treatment was selected because it is known to enhance the SCC susceptibility of Alloy 718. This would help us complete the SCC testing within a reasonable test duration that otherwise could last too long for the program.

Table 4. Chemical composition (wt. %) of Alloy 718 Heat HT6097EK11 in comparison to the Alloy 718 specifications.

Element	A718 Spec	Alloy 718 Heat HT6097EK11
C	<0.08	0.03
Cr	17-21	18.68
Fe	Bal.	17.69
Mn	<0.35	0.09
Ni	50-55	53.53
Mo	2.8-3.3	2.88
Ti	0.65-1.15	0.92
Al	0.2-0.8	0.57
Co	<1	0.22
P	<0.015	0.01
Cu	<0.3	0.12
S	<0.015	0.001
Si	<0.25	0.08
Nb+Ta	4.75-5.5	5.04 (Nb: 5.03, Ta: 0.004)
B	/	0.002
Bi	/	0.000019
Pb	/	0.00008

3.2.2 Characterizations of the Alloy 718 Material

After the precipitation hardening treatment, hardness measurements and material characterizations were performed on the "A", "B", and "C" observation directions to evaluate the mechanical properties and microstructures. The samples were polished to a colloidal silica finish that removed all the hardened damage layer produced during machining. The hardness measurements were carried out on a CM-700AT Clark Microhardness Tester equipped with a FutureTech FM-ARS9000 fully automated hardness testing system. A 3×3 array of indents was acquired on each sample using a load of 300 g, an indent spacing of 0.225 mm (maintains >3d spacing between the indents), and a dwell time of 12 s. These parameters were chosen following our standard procedure for measuring hardness on Ni-base alloys [20]. As summarized in Table 5, the results suggest that the precipitation-hardened Alloy 718 material exhibits a similar average hardness between ~430-445 HV in all planes, which meets the post-heat treatment hardness criteria (>342 HV) specified in SAE AMS5663.

Table 5. Vickers hardness measured on the "A", "B", and "C" observation planes of the precipitation-hardened Alloy 718 (heat number HT6097EK11).

	"A" plane	**"B" plane**	**"C" plane**
Hardness (HV)	427.20±3.69	445.57±10.67	433.05±14.79

The samples were then etched using the same etching procedure as the one used for the Alloy X-750 optical examinations. The results are shown for each observation direction in Figures 20-22. anisotropic shape grains with a long axis aligned to the longitudinal direction were found when viewing the microstructure from the "A" direction where the S-plane can be seen in cross-section and the L-plane normal corresponds to the plate processing direction (Figure 20). While some variation exists in grain size between <100 to ~200 μm, no obvious banding was observed in this material. SEM examinations and EDS analysis were also performed on non-etched samples to evaluate precipitate types and their distribution. As shown in Figures 23 and 24, stringers of intragranular coarse (Nb, Ti)C carbides and TiN carbonitrides were occasionally found along the processing direction in the "A" observation direction. In some cases, NbC-type carbides are seen to nucleate on the TiN carbonitrides (Figure 25, middle image). Figures 23 and 25 also revealed a semi-continuous distribution of sub-micrometer to a few micrometer-sized, thin platelet-like secondary phase precipitates on the majority of the high-energy grain boundaries and some prior grain boundaries. Their bright contrast in the SEM-BSE images and enrichment in Nb are consistent with the δ phase that is a common feature in precipitation-hardened Alloy 718 [17]. In addition, much finer, 10s–100s of nanometer-sized $Cr_{23}C_6$ type precipitates were found to be frequently dispersed along the high-energy grain boundaries adjacent to the δ phases. An example is provided in Figure 26, where high content of Cr was observed at several locations coincident with the darker-contrasted precipitates in the corresponding SEM BSE image.

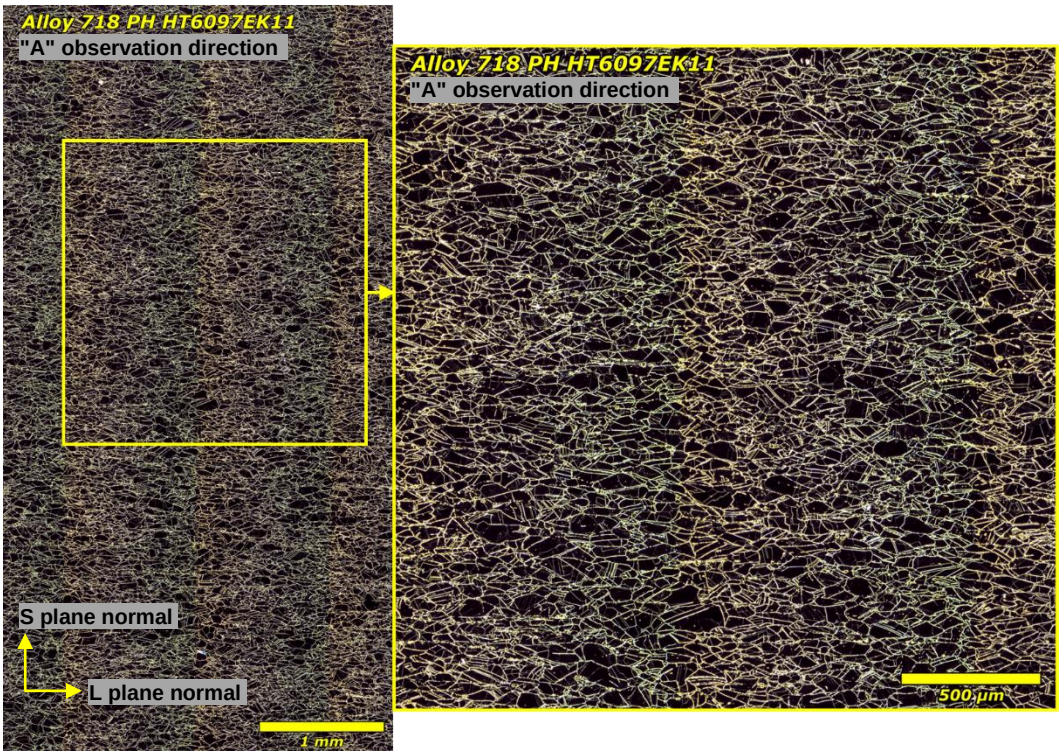

Figure 20. Representative optical micrograph of the microstructure revealed in the "A" observation direction of the precipitation-hardened (PH) Alloy 718 material (heat HT6097EK11).

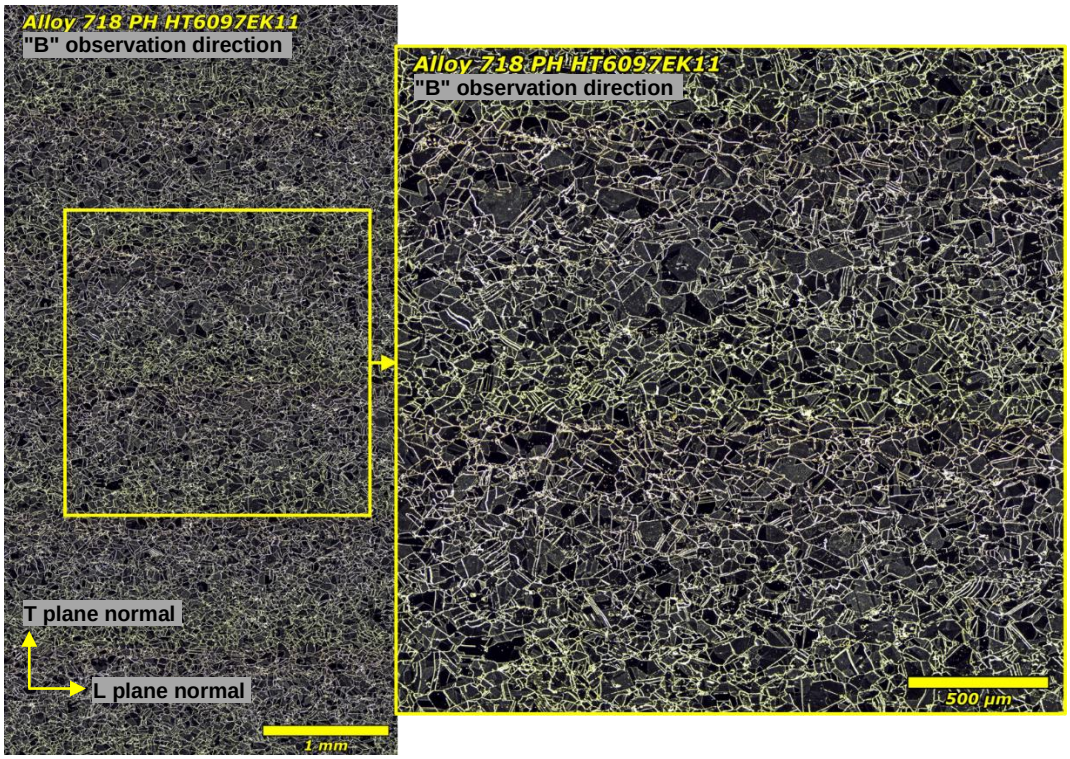

Figure 21. Representative optical micrograph of the microstructure revealed in the "B" observation direction of the Alloy 718PH material (heat HT6097EK11).

Figure 22. Representative optical micrograph of the microstructure revealed in the "C" observation direction of the Alloy 718PH material (heat HT6097EK11).

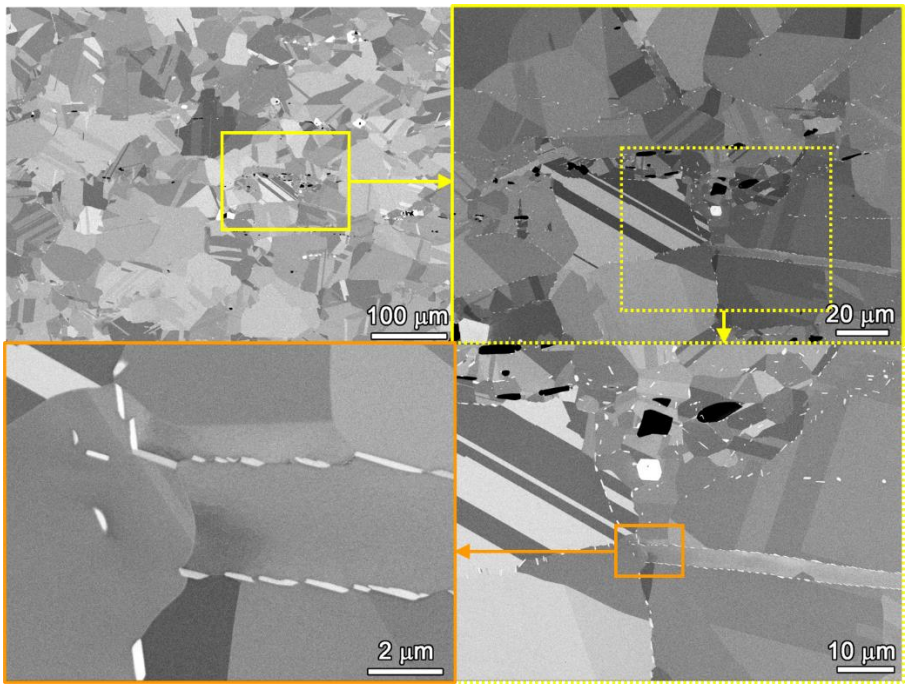

Figure 23. SEM-BSE images of larger precipitates on grain boundaries in the "A" observation direction of the Alloy 718PH material (heat HT6097EK11).

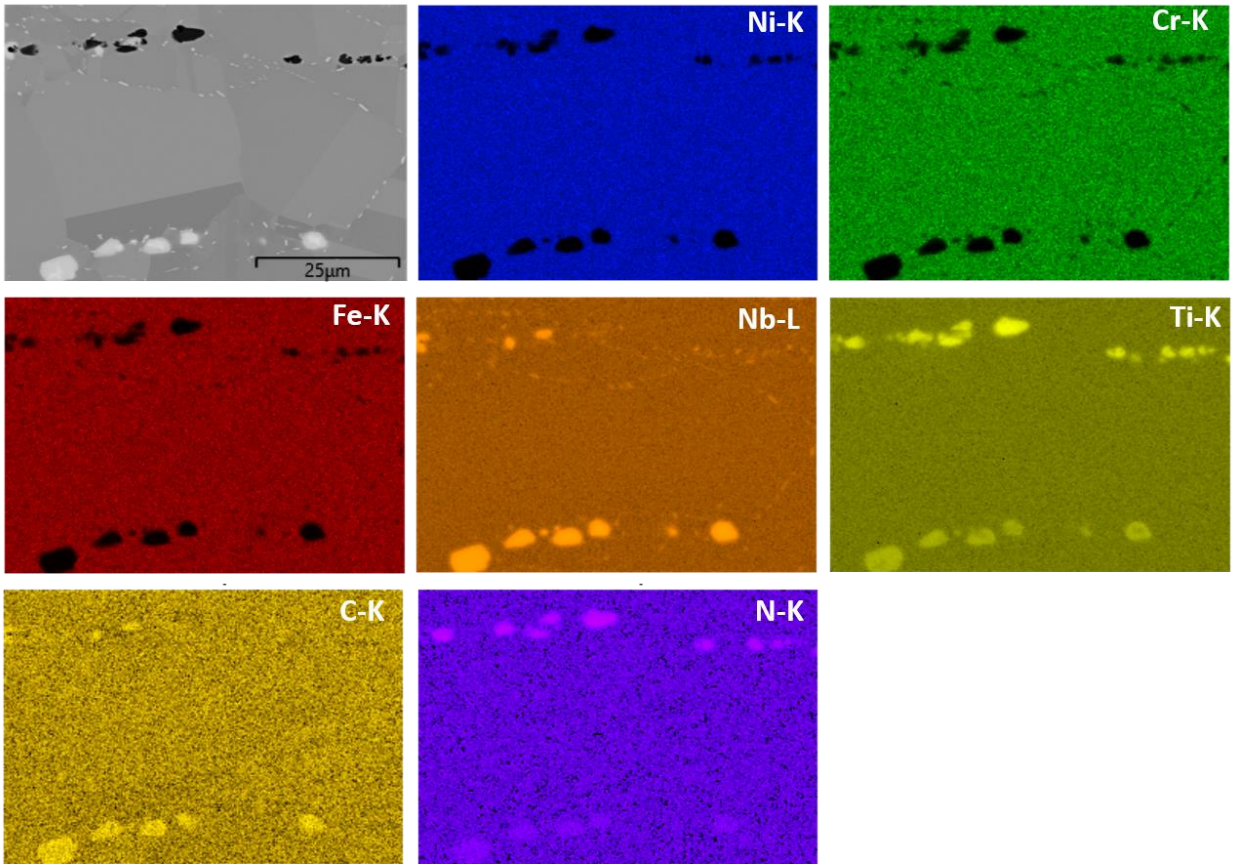

Figure 24. Qualitative SEM-EDS analysis of the chemical composition of the precipitates observed in the "A" observation direction of the Alloy 718PH material (heat HT6097EK11).

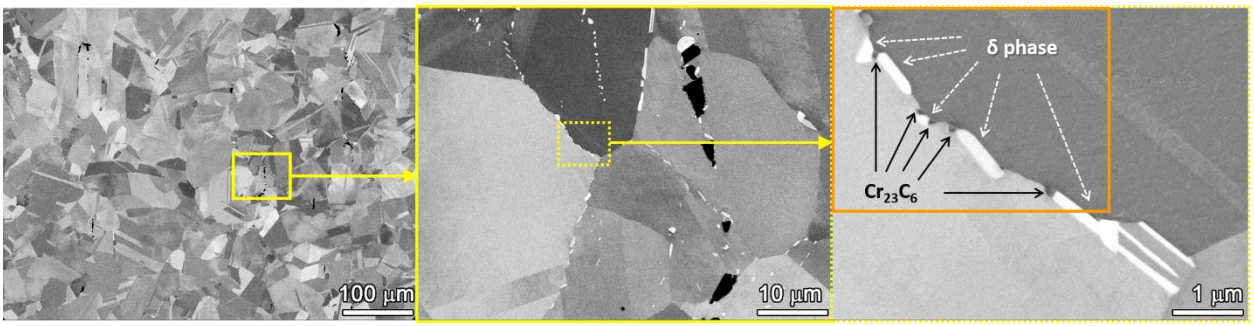

Figure 25. SEM-BSE images of larger precipitates on grain boundaries in the "B" observation direction of the Alloy 718PH material (heat HT6097EK11).

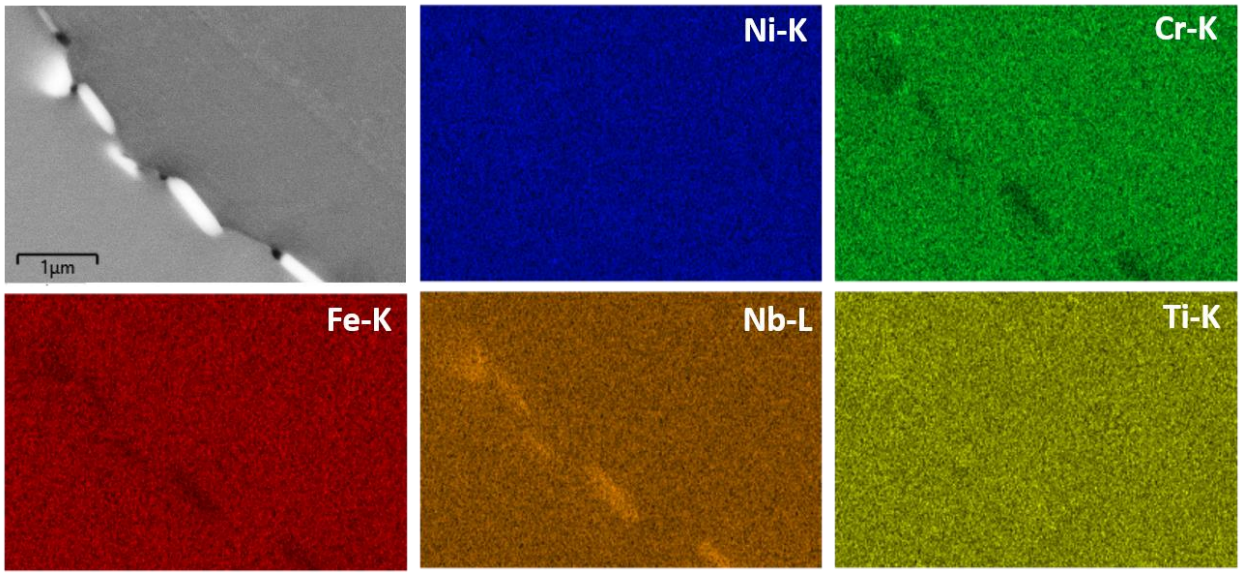

Figure 26. Qualitative SEM-EDS analysis of the chemical composition of the region highlighted in the orange box in the far-right image of Figure 25.

4. TEST RESULTS OF Alloy X-750 IN KOH VS. LIOH-CONTAINING PWR PRIMARY WATER

4.1 Specimen Preparation

As shown in Section 3.1.2, the Alloy X-750 material features substantial banding along the processing direction. The banded regions contain a high density of both intragranular and IG primary and secondary carbides. These carbides are excellent void nucleation sites that can contribute to planar fracture in cases where they are in a plane aligned perpendicular to the tensile axis. This suggests a higher SCC susceptibility for cracking along the banded plane. As a result, the T-L orientation relative to the processing direction was chosen for the evaluation of SCC growth behavior of the Alloy X-750 material. In this way, the primary SCC cracking will not take place in the microstructural banding, and more uniform crack growth behavior is expected. However, based on prior experience, some branch cracking on the orthogonally oriented banding planes may occur, but this will have little or no effect of SCC growth in the target cracking plane. The corresponding orientation of the 0.5T CT specimens in the Alloy X-750 block is shown in Figure 27. In addition, twelve initiation specimens (six for KOH and six for LiOH) were extracted from the same block as shown in the same figure. This configuration positions the axial direction of the specimens along the transverse direction and the radial direction of the specimens coincident with the normal vector to the banding plane. For both the SCC initiation and growth rate tests, the Alloy X-750 specimens were tested in as-received condition with no further heat treatment or cold work.

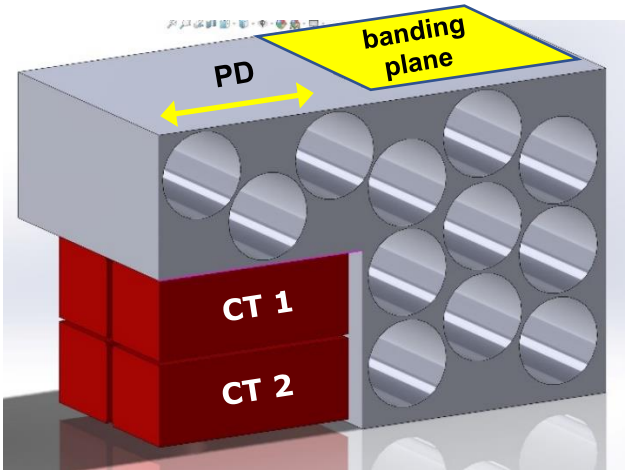

Figure 27. Schematic illustrating the orientation of the twelve initiation specimens and two CT specimens in the Alloy X-750 block. PD = processing direction.

4.2 SCC Initiation Behavior of Alloy X-750 in KOH vs. LiOH-Containing PWR Primary Water

4.2.1 Test Procedure and DCPD Response

Six Alloy X-750 specimens were tested in each of the two medium-size LWRS test systems. This is the maximum quantity that can fit in these test systems, and while six specimens are insufficient for any definitive statistical analysis of the initiation behavior, this quantity will provide some insight into the distribution of initiation times. The tests were performed in 360°C water with a dissolved hydrogen content of 26 cc/kg to maintain an electrochemical corrosion potential at the Ni/NiO stability line, where the SCC initiation susceptibility is believed to be the highest for Ni-base alloys. The water chemistry in these two systems represents the BOC water chemistry as specified in Table 1 with 1500 ppm B as H_3BO_3 and either 2.2 ppm Li as LiOH or 12.4 ppm K as KOH.

The target test stress is the 0.2% offset YS of the material. As described in Section 2.1, PNNL tracks the stress versus strain response of all six specimens during the specimen loading process, often with a resolution of 0.01% plastic strain, allowing us to precisely measure the plastic strain of each specimen. The loading of these specimens began within 1–2 days after the systems reached the target test temperature and water chemistry, and the target load was achieved over a period of 1–2 hours at a constant strain rate of ~1×10^{-5} s^{-1}. The initial loading run in the two sets of specimens is presented in Figure 28 for the reference LiOH BOC water chemistry and Figure 29 for the KOH BOC water chemistry, respectively. Due to intrinsic differences in microstructure and/or gauge diameters, there is always some variability in the attained plastic strain among the specimens. PNNL attempts to ensure that the majority of the specimens reach 0.2% plastic strain and tries to not allow any specimens to have less than 0.15% plastic strain. During the constant load observation period, both tests were interrupted multiple times to remove initiated specimens. The remaining specimens were then reloaded to their original load following the same procedure. Additional plastic strain was sometimes incurred during reloading the specimens (this is commonly observed for many materials that PNNL has SCC initiation tested) and was recorded to calculate the total plastic strain for each specimen upon completion of the test. The data is shown in Table 6 together with other test status information, including the SCC initiation time of all specimens.

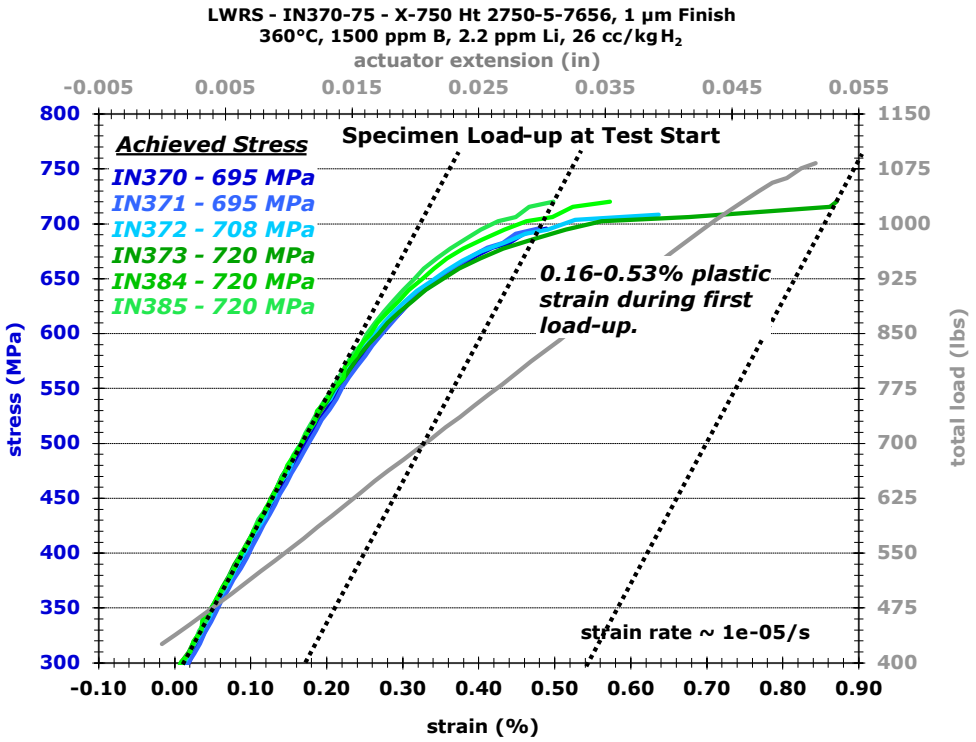

Figure 28. The stress vs. strain plot during the initial loading of the six Alloy X-750 specimens IN370-75 in 360°C PWR primary water containing 1500 ppm B and 2.2 ppm Li.

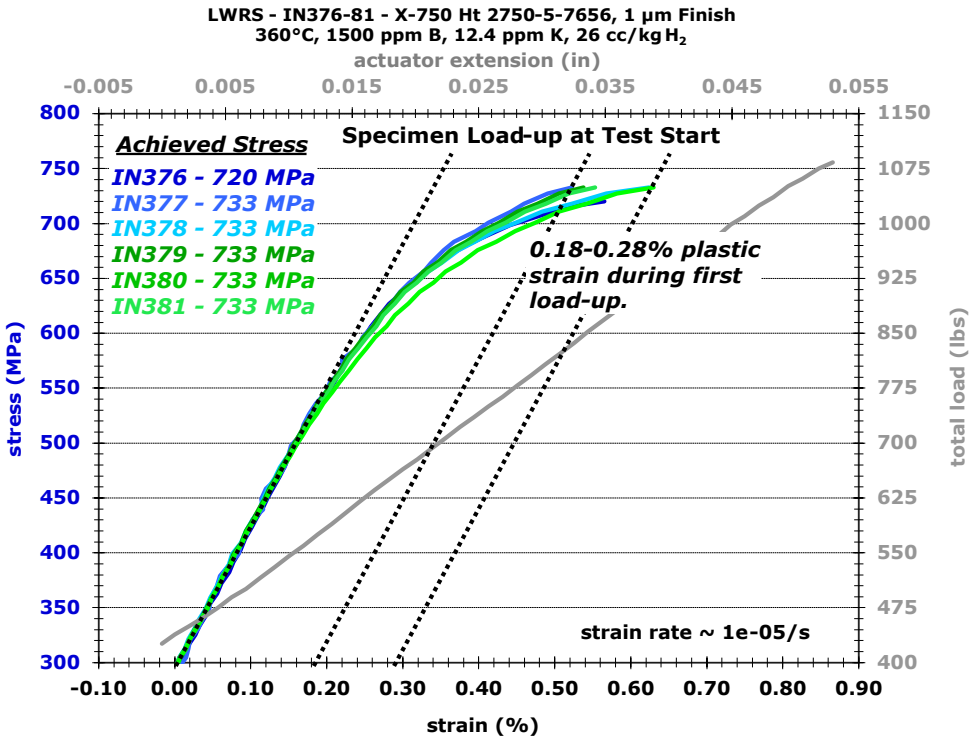

Figure 29. The stress vs. strain plot during the initial loading of the six Alloy X-750 specimens IN376-81 in 360°C PWR primary water containing 1500 ppm B and 12.4 ppm K.

Table 6. Summary of the SCC initiation test status of the Alloy X-750 Heat 2750-5-7656.

Spec. ID	ppm B, ppm Li, or ppm K	Finish	Temp (ºC)	Applied Stress (MPa)	Total accumulated plastic strain (%)	Time to SCC initiation (h)
IN370	1500 B/2.2 Li	1 µm	360	695	0.22	660
IN371	1500 B/2.2 Li	1 µm	360	695	0.29	857
IN372	1500 B/2.2 Li	1 µm	360	708	0.31	185
IN373	1500 B/2.2 Li	1 µm	360	720	0.57	550
IN374	1500 B/2.2 Li	1 µm	360	720	0.28	1257
IN375	1500 B/2.2 Li	1 µm	360	720	0.40	1077
IN376	1500 B/12.4 K	1 µm	360	720	0.39	NI (1714)*
IN377	1500 B/12.4 K	1 µm	360	733	0.18	288
IN378	1500 B/12.4 K	1 µm	360	733	0.34	817
IN379	1500 B/12.4 K	1 µm	360	733	0.33	899
IN380	1500 B/12.4 K	1 µm	360	733	0.30	658
IN381	1500 B/12.4 K	1 µm	360	733	0.28	370

*NI = no initiation. The time in the parenthesis indicates the total exposure time of the specimen when the test was ended.

An overview of the referenced DCPD strain response for the six specimens tested in the LiOH and KOH BOC water chemistries is presented in Figures 30 and 31, respectively. SCC initiation is considered to take place when an obvious increase in strain rate occurs in the referenced DCPD strain response as highlighted for each specimen in these figures. In general, all tested specimens in both water chemistries initiated within ~1,200 hours of exposure with only one exception (IN376). These initiation times are slightly higher and have a greater spread in times than observed for individual heats 15% CF Alloy 600 heats that have a YS of ~500-550 MPa [21, 22], suggesting that Alloy X-750 is slightly more resistance to SCC initiation than 15% CF Alloy 600.

When comparing response between KOH and LiOH water chemistries, it can be seen that one specimen (IN372) among the six specimens tested in the LiOH BOC water chemistry showed relatively early initiation at 185 hours, while the other five initiated between 550–1,257 hours. The specimens tested in the KOH BOC water chemistry showed a slightly tighter band with five initiations between 288–899 hours, but no indication of SCC initiation was found on the remaining specimen IN376 by the time the test was stopped due to a scheduled building maintenance outage at 1,714 hours.

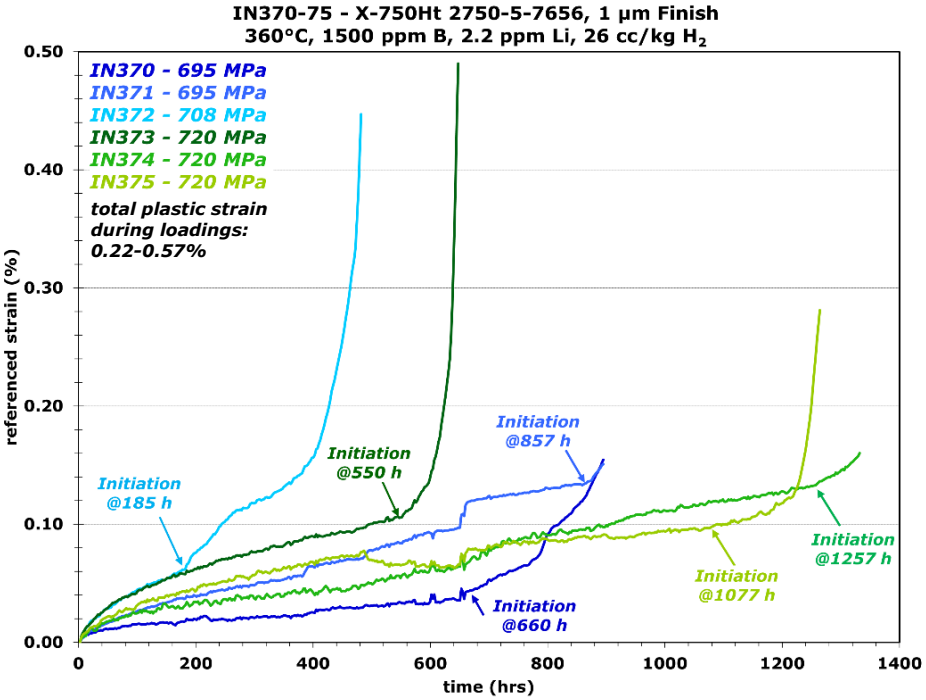

Figure 30. Overall referenced DCPD strain response of the six Alloy X-750 specimens IN370-75 tested at material yield stress in 360°C PWR primary water containing 1500 ppm B and 2.2 ppm Li. The SCC initiation time of each specimen is marked in the plot.

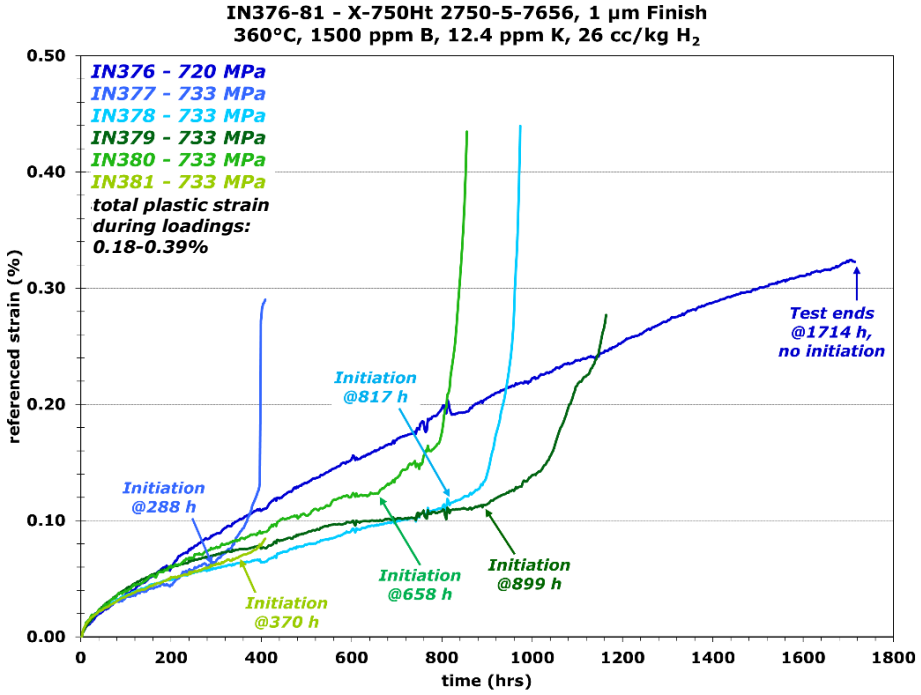

Figure 31. Overall referenced DCPD strain response of the six Alloy X-750 specimens IN376-81 tested at material yield stress in 360°C PWR primary water containing 1500 ppm B and 12.4 ppm K. Except IN376 (no initiation by the time the test ended at 1714 hours), the SCC initiation times of all specimens are marked in the plot.

The SCC initiation times acquired from both test systems were also plotted as a function of total plastic strain and applied stress as shown in Figures 32 and 33, respectively. No systematic trend in SCC initiation behavior was revealed between KOH and LiOH for this analysis approach. A Weibull analysis of the SCC initiation data was also performed on the two data sets. A standard Weibull analysis was performed on the LiOH BOC data while a censored Weibull analysis was performed on the KOH BOC data set that had one non-initiated specimen. A detailed description of the censored Weibull approach as it pertains to SCC initiation data with non-initiated values is presented in Reference [22]. Graphical results are shown in Figure 34 for the LiOH BOC water chemistry and in Figure 35 for the KOH BOC water chemistry. As noted in the plots, a characteristic time (corresponding to 63% of initiations occurring) of 861 hours was found for the LiOH test and 967 hours for the KOH test. The mean initiation time in Table 7 is also slightly longer for KOH than for LiOH. While large overlap exists in the 95% confidence interval of a cumulative failure probability of 10%, 50%, and 90% between these two water chemistries, these data also indicate that the SCC initiation time of Alloy X-750 in the KOH BOC may be slightly longer than in the LiOH BOC environment.

The key contributor to this trend is the non-initiated specimen in the KOH BOC water chemistry that withstood ~27–90% longer exposure time than the specimens tested in the LiOH BOC water chemistry. When taking this into account, the trend for a slightly longer SCC initiation time in KOH water chemistry could be considered due to intrinsic microstructural inhomogeneities among the 12 specimens and is within statistical error. The most important outcome of this testing is that the SCC initiation times measured in KOH BOC water chemistry and the reference LiOH BOC water chemistry fall well within the same range, suggesting that using KOH instead of LiOH would not result in an adverse effect on SCC initiation of Alloy X-750.

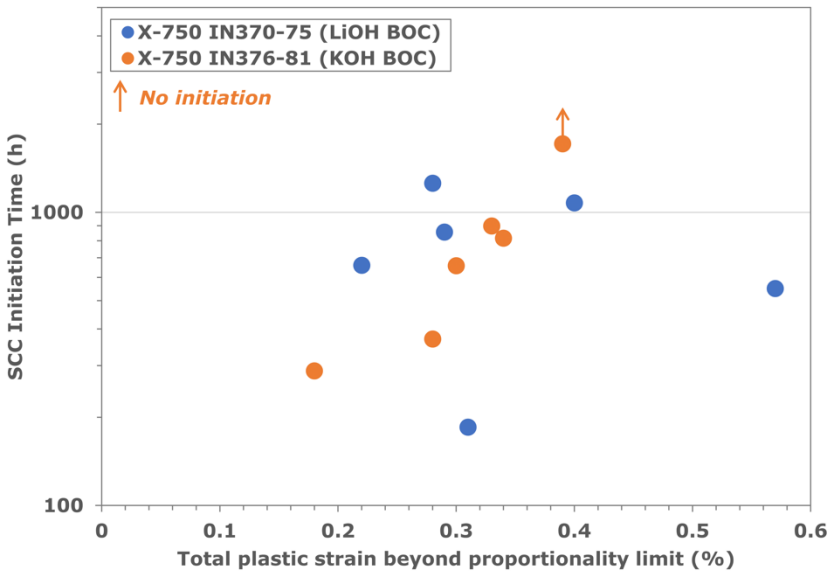

Figure 32. SCC initiation time of all the tested Alloy X-750 specimens as a function of total plastic strain accumulated in them during every loading run.

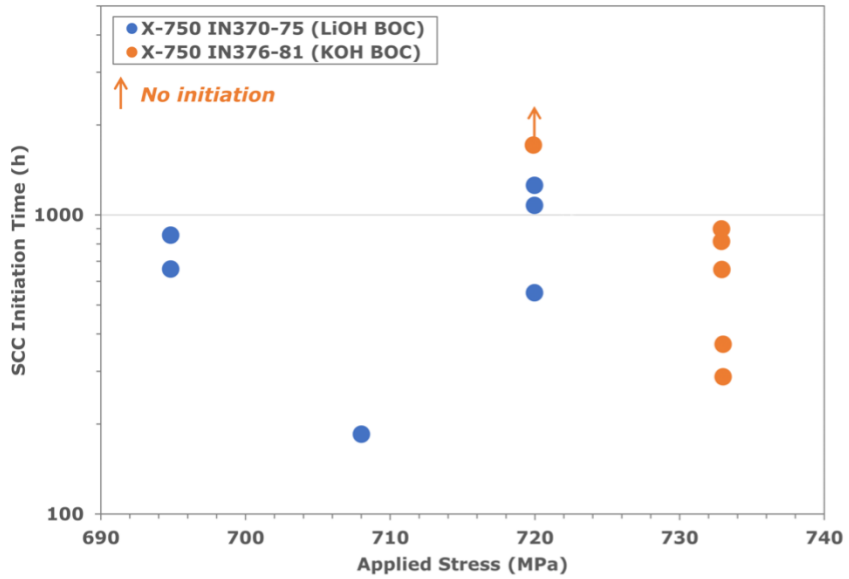

Figure 33. SCC initiation time of all the tested Alloy X-750 specimens as a function of applied stress (i.e., yield stress).

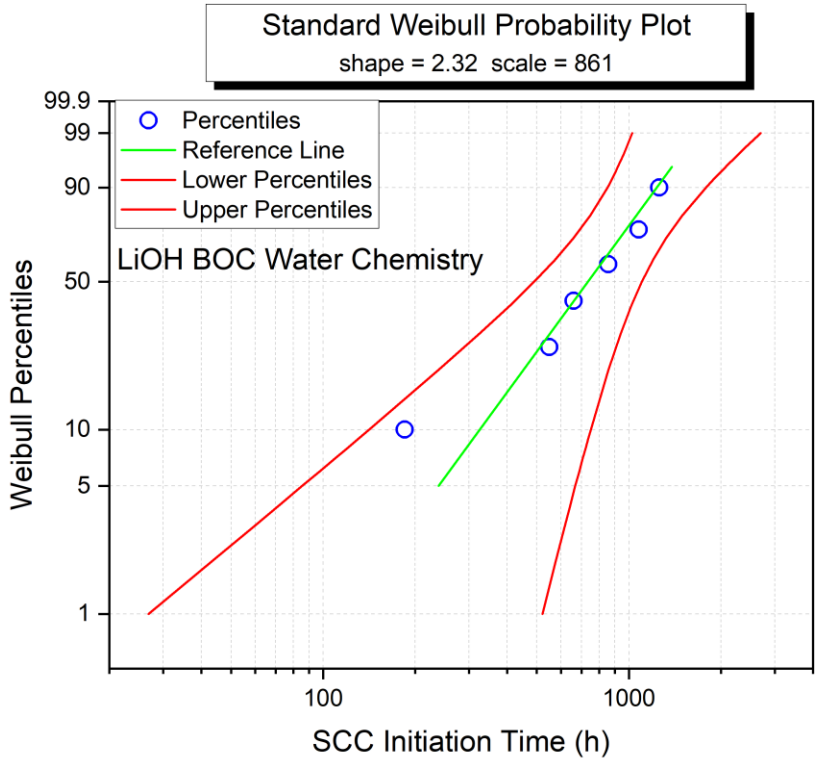

Figure 34. Standard Weibull analysis (cumulative failure vs. hours) with a 95% confidence interval based on the SCC initiation times acquired on Alloy X-750 at yield stress in 360°C water with 1500 ppm B and 2.2 ppm Li. All six specimens have initiated and are considered failures in this analysis.

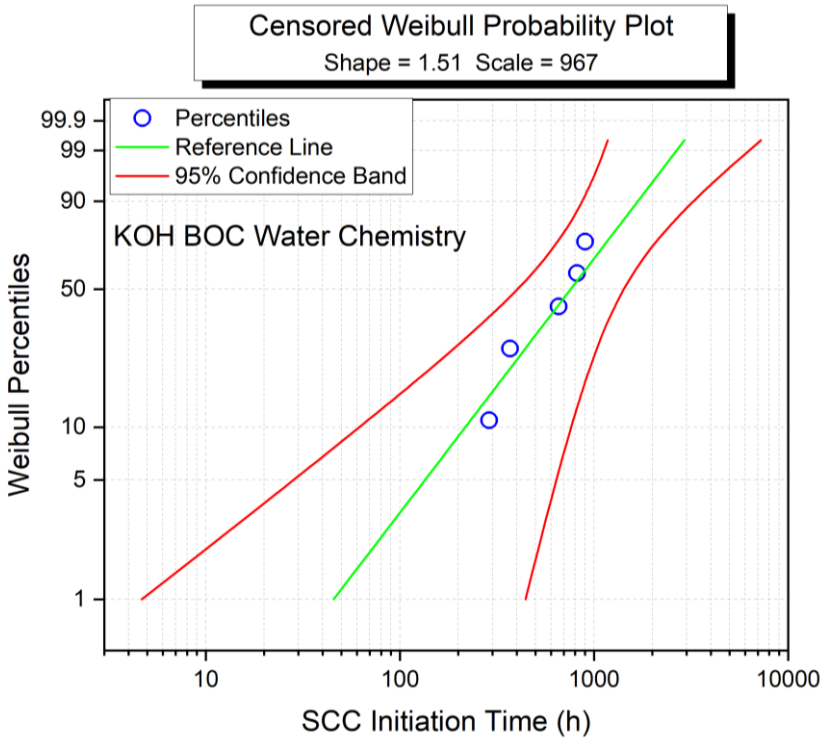

Figure 35. Censored Weibull analysis (cumulative failure vs. hours) with a 95% confidence interval based on the SCC initiation times acquired on Alloy X-750 at yield stress in 360°C water with 1500 ppm B and 12.4 ppm K. Five out of the six specimens have initiated and are considered failures in this analysis. This censored analysis also accounts for the one non-failure event.

Table 7. Mean, standard deviation, and failure times at lower and upper 95% confidence intervals for 10%, 50%, and 90% cumulative failures of Alloy X-750. Mean and standard deviation for the KOH water chemistry were calculated with the inclusion of the non-initiated value.

Water Chemistry, ppm	Mean	Std Dev	10% Failures	50% Failures	90% Failures
1500 B, 2.2 Li	764	352	~141–750 h	~490–1,102 h	~851–1,789 h
1500 B, 12.4 K	791	468	~62–762 h	~403–1,424 h	~869–3,257 h

4.2.2 Post-Test Cracking Morphology

The main goal of the post-test SEM characterization on the initiated specimens is to examine whether any obvious difference is present in the initiation morphology of the specimens tested in the KOH vs. LiOH BOC water chemistries. When specifically studying SCC initiation crack morphology, PNNL stops a test immediately after SCC initiation is detected in a specimen to allow examination of the crack morphology at the time of initiation. However, because the primary goal of this KOH vs. LiOH SCC initiation study is to measure SCC initiation time, the tests were only interrupted when a specimen was nearing failure. This allows for the chance of having multiple specimens initiate before a test interruption is needed, reducing the number of test interruptions, and making more effective use of time and project funds. In the following sections, the SCC initiation morphology of the specimens tested in the LiOH and the KOH BOC water chemistries will be presented and compared in detail.

4.2.2.1 SCC Initiation Morphology in the LiOH BOC Water Chemistry

The post-test surface morphology of the six Alloy X-750 specimens IN370–75 tested in the LiOH BOC water chemistry are presented in Figures 36–41. The specimens are reported in order of increasing SCC initiation time. The loading direction was parallel to the axial direction of the specimens which is left-to-right in the figures. For each specimen, obvious cracks are highlighted in red in the montaged image. The primary crack(s) that are considered responsible for DCPD detection of SCC initiation are also shown at higher magnifications in the same figure. As shown in Figure 30, many specimens (IN372, 373, 375, and 376) were exposed in water for ~100 hours or more after SCC initiation was confirmed and exhibited a very high strain rate before they were taken out. However, very few (<10) cracks were identified, among which usually only one or two exhibited a much longer length and wider opening than the others. Meanwhile, the majority of the specimen surface appears to be intact from IG oxidation or cracking. These observations are very different from our experience with Alloy 600 and Alloy 182, which could exhibit extensive IG oxidation and cracking all over the specimen surface after similar exposure times. This distinct initiation cracking morphology is therefore an indication of non-uniform sensitivity to IG corrosion and crack nucleation in Alloy X-750, in which cracks can develop relatively quickly in regions with high susceptibility to IG failure. As shown in Figures 14–16, the Alloy X-750 material features extensive grain size and carbide banding. The large grains have a size of ~200 μm or more, whereas the fine grains are typically well below 100 μm. Judging from the tortuous IG morphology along a length of a few hundred of micrometers revealed by the primary cracks in most samples, one possibility is that SCC initiation in this material is occurring in the fine-grained banded microstructure. As can be deduced from Figure 27, the banding planes run along the length of the specimen, and the guillotine cracks that are forming could intersect a banding plane. However, further investigations, such as cross-section examination or a second SEM surface examination after the specimens are etched, are needed to confirm this hypothesis.

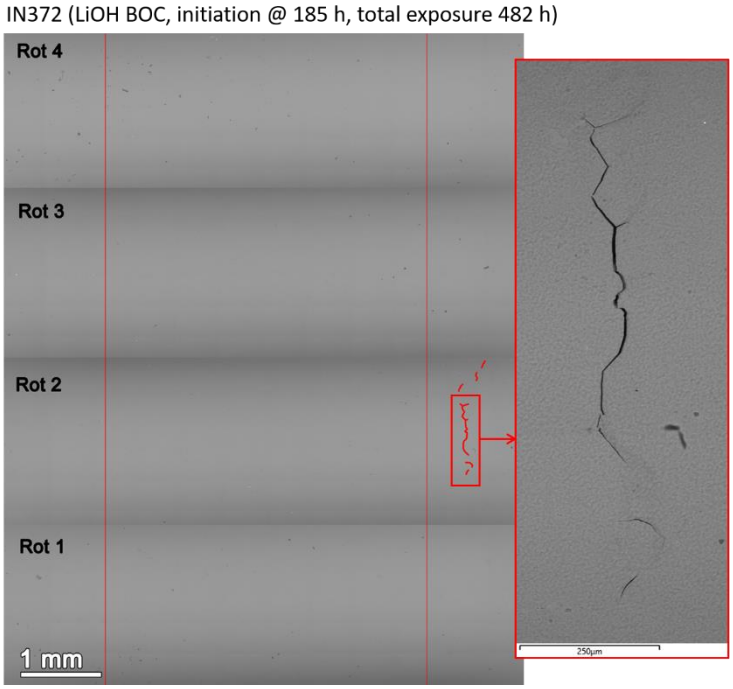

Figure 36. Post-test SEM-BSE montage of the first initiated specimen IN372 in 360°C PWR primary water with 1500 ppm B and 2.2 ppm Li. Obvious cracks are highlighted in red and the primary crack(s) responsible for DCPD detection of SCC initiation are shown at higher magnifications.

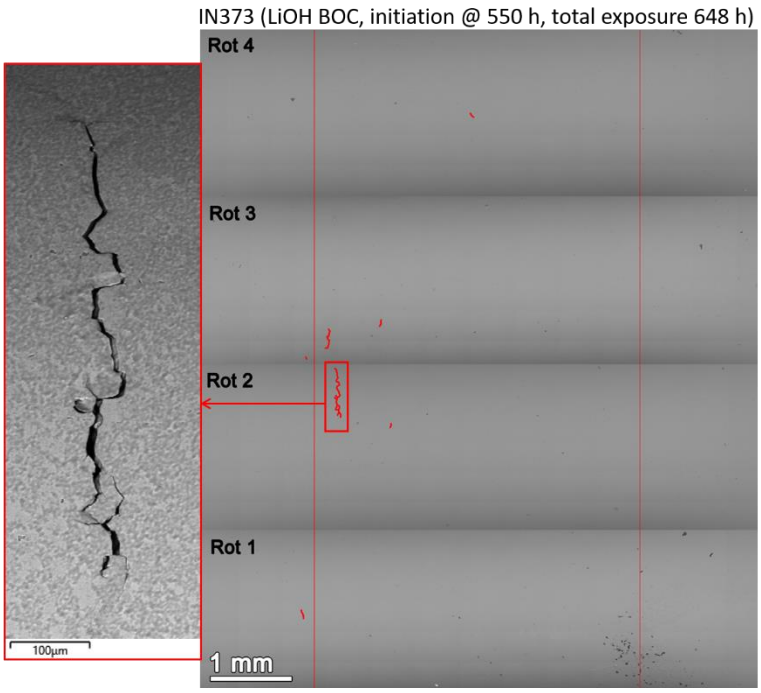

Figure 37. Post-test SEM-BSE montage of the second initiated specimen IN373 in 360°C PWR primary water with 1500 ppm B and 2.2 ppm Li. Obvious cracks are highlighted in red. The primary crack(s) responsible for DCPD detection of SCC initiation are shown at higher magnifications.

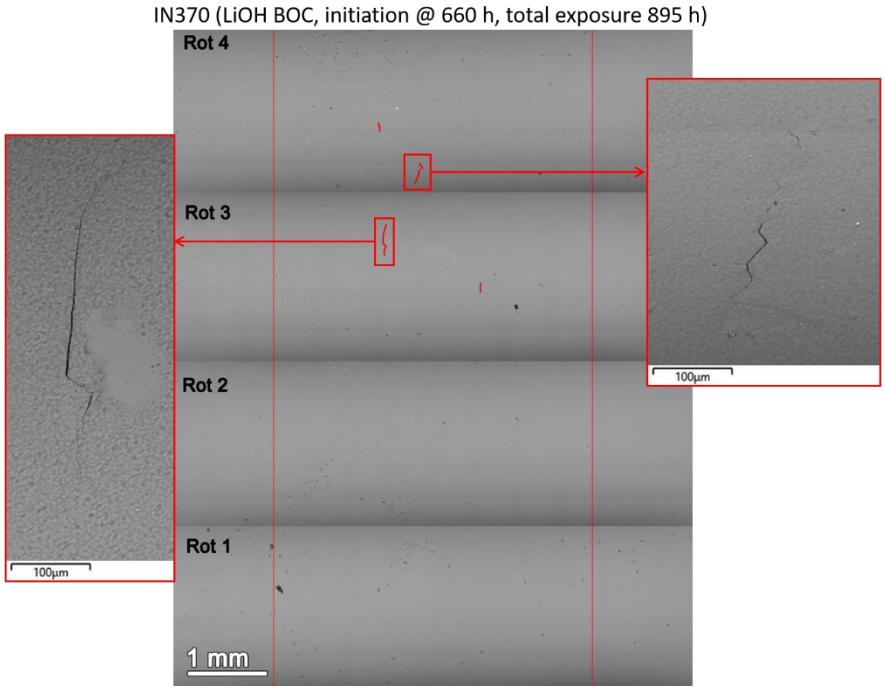

Figure 38. Post-test SEM-BSE montage of the third initiated specimen IN370 in 360°C PWR primary water with 1500 ppm B and 2.2 ppm Li. Obvious cracks are highlighted in red. The primary crack(s) responsible for DCPD detection of SCC initiation are shown at higher magnifications.

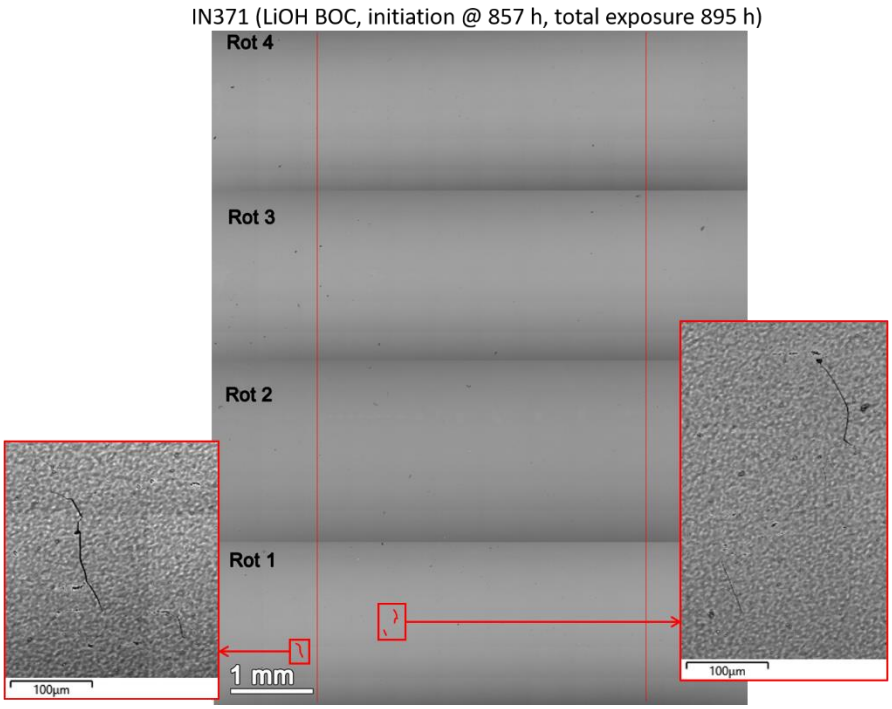

Figure 39. Post-test SEM-BSE montage of the fourth initiated specimen IN371 in 360°C PWR primary water with 1500 ppm B and 2.2 ppm Li. Obvious cracks are highlighted in red. The primary crack(s) responsible for DCPD detection of SCC initiation are shown at higher magnifications.

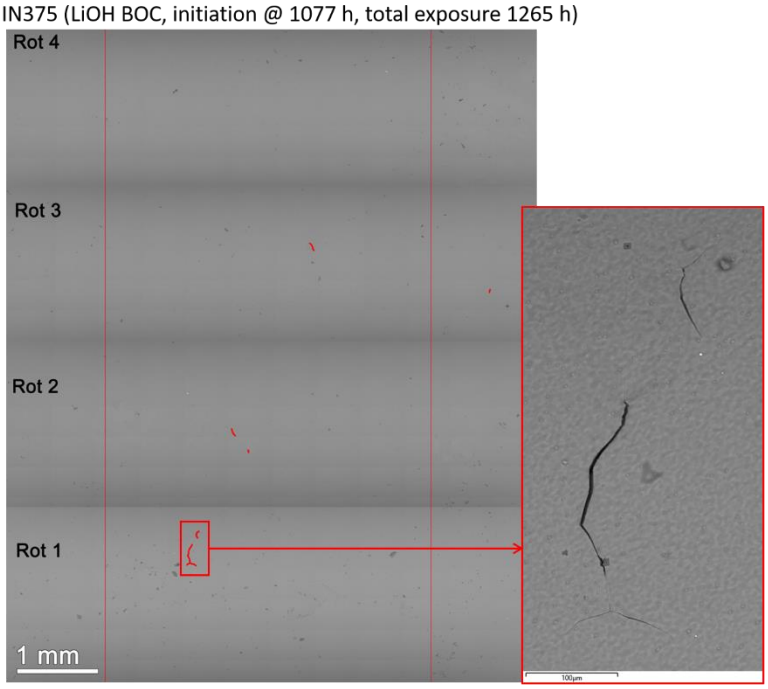

Figure 40. Post-test SEM-BSE montage of the fifth initiated specimen IN375 in 360°C PWR primary water with 1500 ppm B and 2.2 ppm Li. Obvious cracks are highlighted in red. The primary crack(s) responsible for DCPD detection of SCC initiation are shown at higher magnifications.

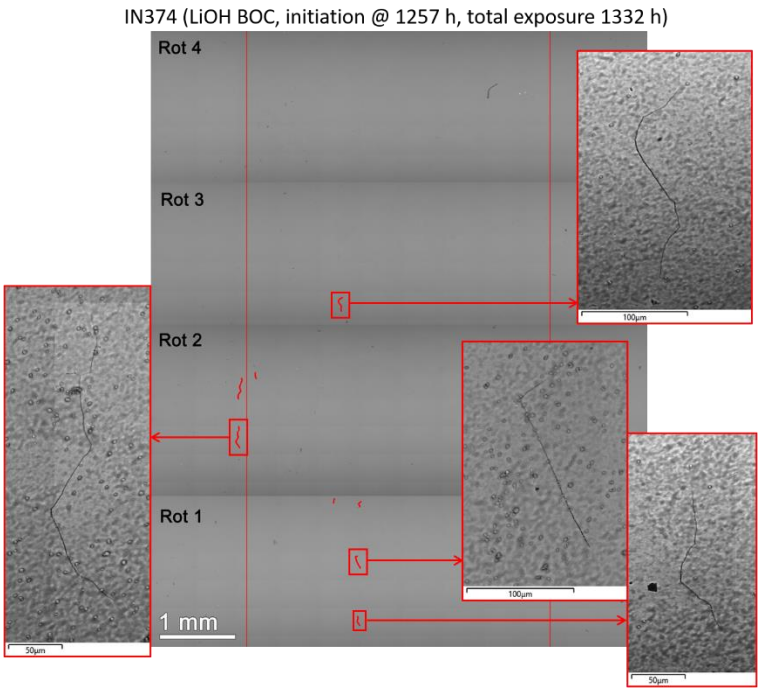

Figure 41. Post-test SEM-BSE montage of the last (sixth) initiated specimen IN374 in 360°C PWR primary water with 1500 ppm B and 2.2 ppm Li. Obvious cracks are highlighted in red with a few examples shown at higher magnifications.

4.2.2.2 SCC Initiation Morphology in the KOH BOC Water Chemistry

The post-test surface morphology of the five initiated Alloy X-750 specimens IN377–81 tested in the BOC water chemistry containing 1500 ppm B and 12.4 ppm K are presented in Figures 42–46. These specimens are also reported in order of increasing SCC initiation time, and the loading direction was parallel to the axial direction of the specimens. Like most specimens tested in the reference LiOH BOC water chemistry, four out of the five initiated specimens in this test (IN377–80) were exposed in water for >100 hours after SCC initiation was detected, and they only exhibited a very limited number of cracks on the surface. The tortuous IG morphology of the primary cracks observed in these specimens, as shown in Figures 42 and 44–46, also indicates that the cracks had likely nucleated along grain boundaries in the fine-grained banded microstructure. In addition, similar cracking morphology was also found in the specimens removed relatively soon after the detection of SCC initiation in both the LiOH and KOH BOC water chemistries. This can be seen by comparing the post-test surface morphology of IN371 and IN381, tested in the LiOH and KOH BOC water chemistry, respectively. Both were removed ~40 hours after DCPD detected SCC initiation. As presented in Figures 39 and 43, these two specimens exhibit very consistent cracking behavior with two to three tight cracks of ~100–200 μm long on the surface. Based on the above observations, it can be concluded that replacing LiOH with KOH did not result in an obvious difference in the SCC initiation morphology of Alloy X-750.

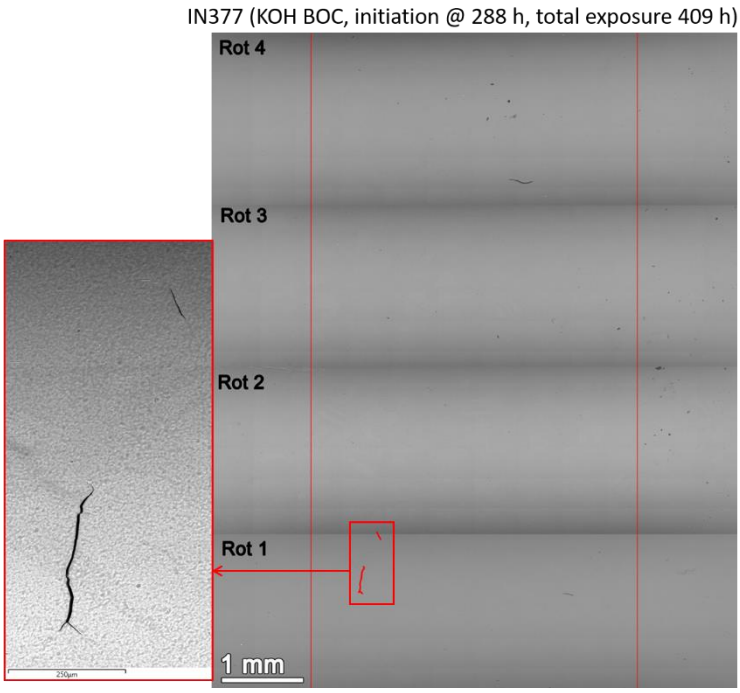

Figure 42. Post-test SEM-BSE montage of the first initiated specimen IN377 in 360°C PWR primary water with 1500 ppm B and 12.4 ppm K. Obvious cracks are highlighted in red. The primary crack(s) responsible for DCPD detection of SCC initiation are shown at higher magnifications.

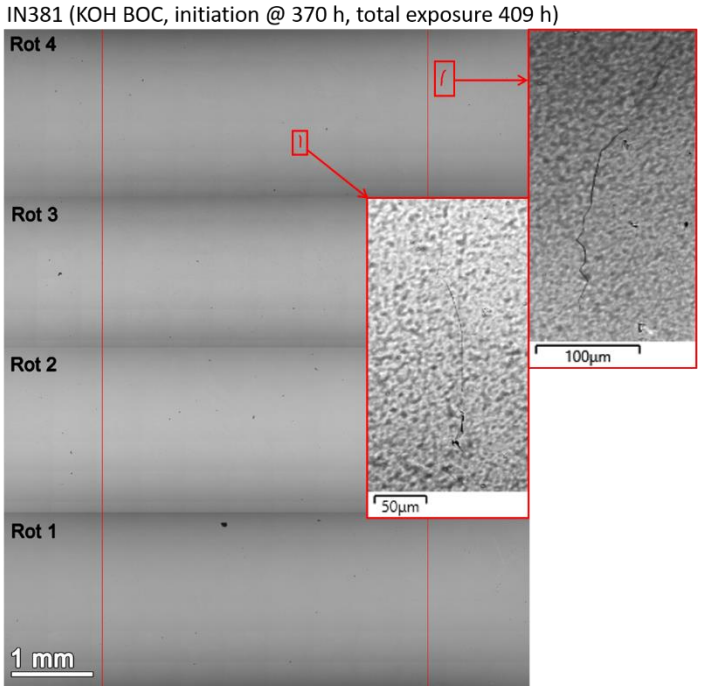

Figure 43. Post-test SEM-BSE montage of the second initiated specimen IN381 in 360°C PWR primary water with 1500 ppm B and 12.4 ppm K. Obvious cracks are highlighted in red. The primary crack(s) responsible for DCPD detection of SCC initiation are shown at higher magnifications.

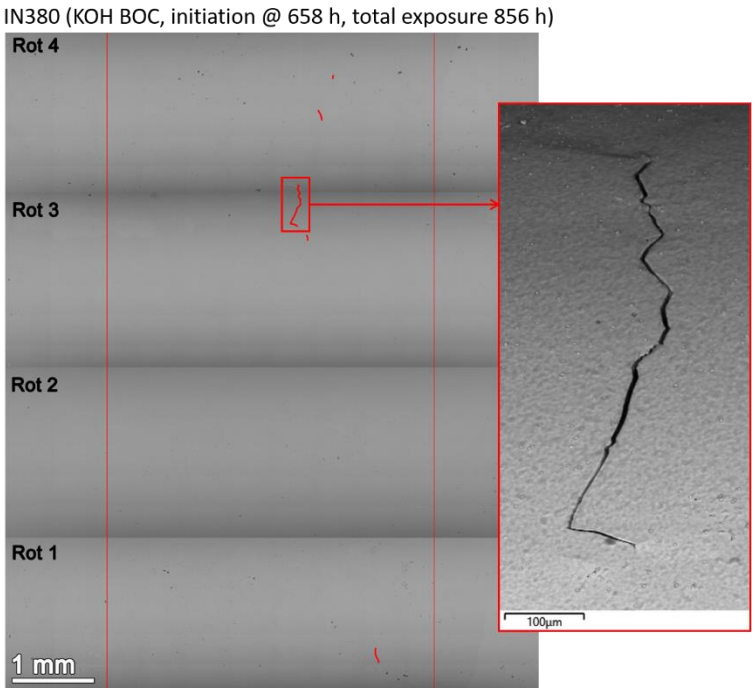

Figure 44. Post-test SEM-BSE montage of the third initiated specimen IN380 in 360°C PWR primary water with 1500 ppm B and 12.4 ppm K. Obvious cracks are highlighted in red. The primary crack(s) responsible for DCPD detection of SCC initiation are shown at higher magnifications.

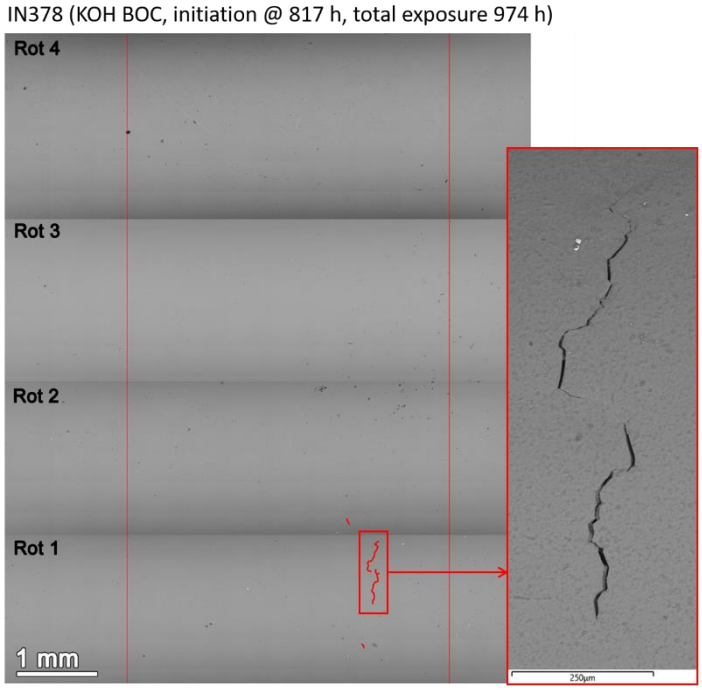

Figure 45. Post-test SEM-BSE montage of the fourth initiated specimen IN378 in 360°C PWR primary water with 1500 ppm B and 12.4 ppm K. Obvious cracks are highlighted in red. The primary crack(s) responsible for DCPD detection of SCC initiation are shown at higher magnifications.

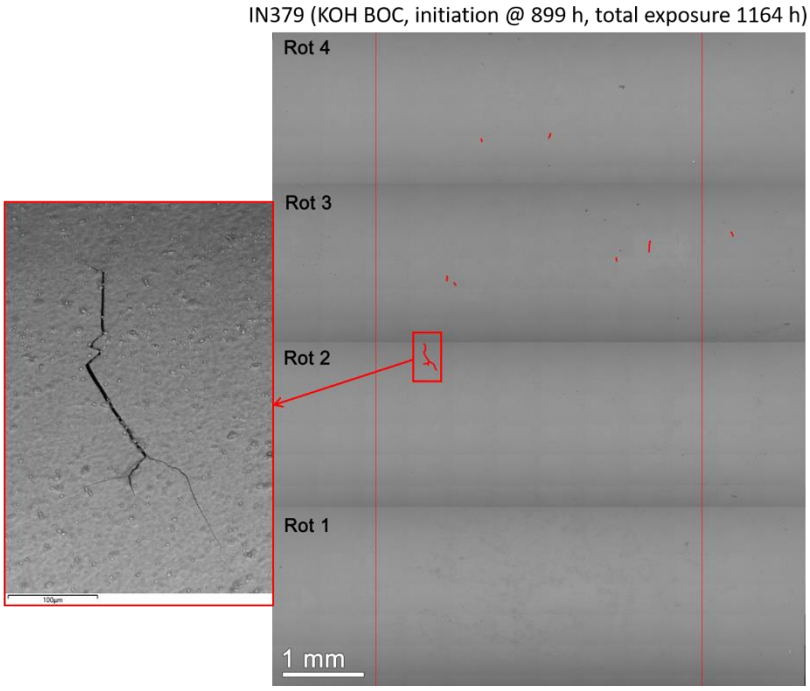

Figure 46. Post-test SEM-BSE montage of the fifth initiated specimen IN379 in 360°C PWR primary water with 1500 ppm B and 12.4 ppm K. Obvious cracks are highlighted in red. The primary crack(s) responsible for DCPD detection of SCC initiation are shown at higher magnifications.

4.3 SCC Crack Growth Behavior of Alloy X-750 in KOH vs. LiOH-Containing PWR Primary Water

This study aims to produce quantitative SCCGR data on Alloy X-750 through in-situ DCPD measurement of cracking in KOH-based water chemistries and corresponding (i.e., same pH(T)) reference LiOH-based water chemistries. The difference in SCCGR between each KOH-based environment and the corresponding LiOH-based reference environment will indicate whether or not the KOH-based water chemistry increases SCC growth susceptibility compared to the reference LiOH-based water chemistry.

Two Alloy X-750 specimens, CT223 and CT224, were first fatigue precracked individually in air at room temperature following the procedure described in Section 2.2.2. The side grooves of these two specimens were polished to a 1 μm finish, allowing the precrack morphology to be viewed and its length to be measured on both sides. In Figures 47 and 48, optical micrographs are provided showing the precrack produced by air fatigue in CT223 and CT224, respectively. While the target precrack length was set at 1.1 mm, the precrack in CT223 exhibited a certain degree of unevenness with a length of 0.605 mm on Side A and a length of 1.506 mm on side B. In comparison, the precrack in CT224 has a more consistent length on both sides (1.185 vs. 1.225 mm). Therefore, it was decided to use CT224 as the controlling sample and CT223 as the companion sample in the SCC growth rate test, meaning that the load control during the test is implemented based on the response of CT224. This helps to guard against the possibility of inaccurate DCPD crack length data causing stress intensity to deviate substantially from the target value.

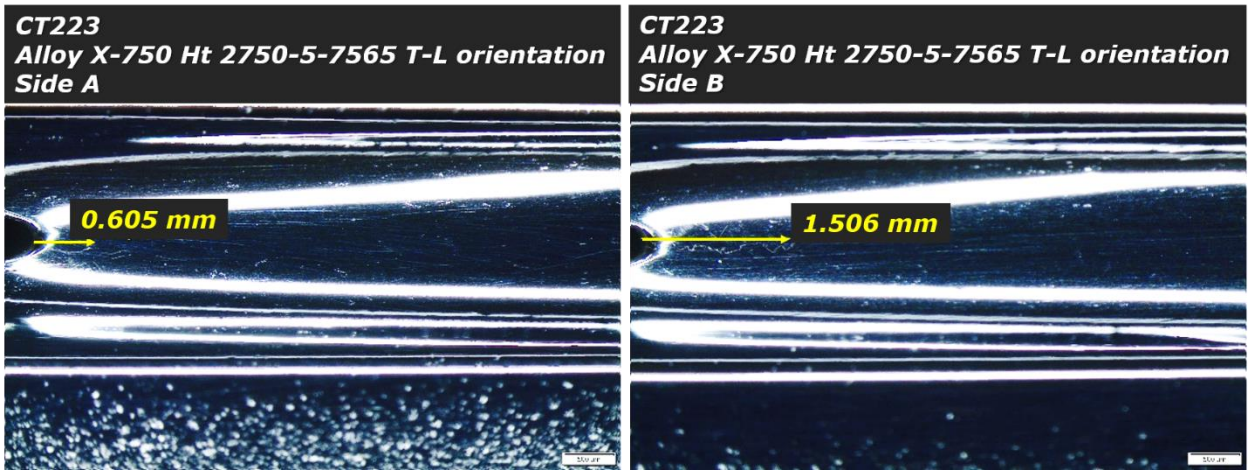

Figure 47. Optical micrographs of the polished side grooves of the Alloy X-750 specimen CT223. The length of the precrack produced by air fatigue is marked in both side grooves.

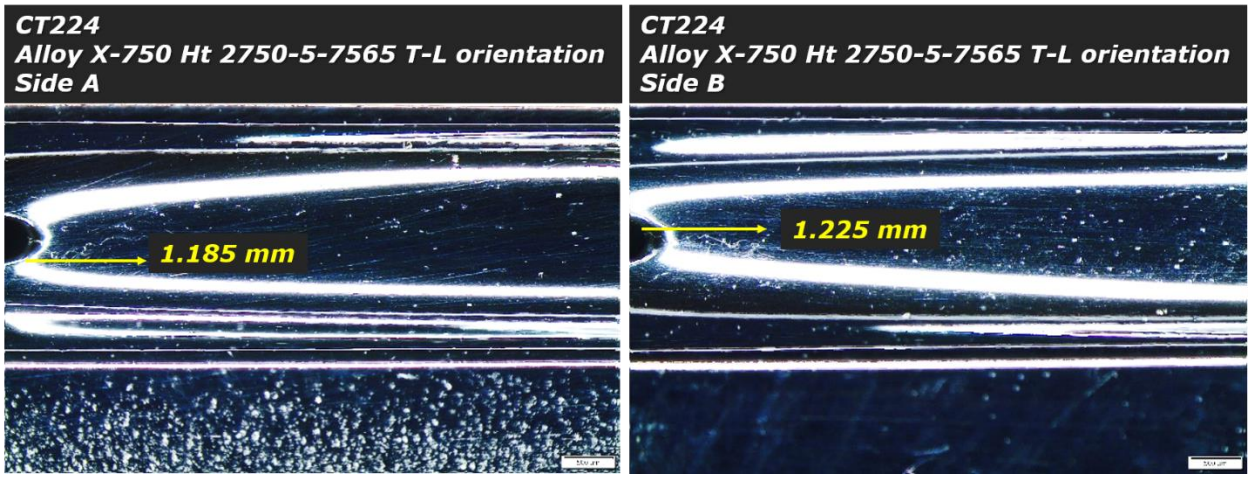

Figure 48. Optical micrographs of the polished side grooves of the Alloy X-750 specimen CT224. The length of the precrack produced by air fatigue is marked in both side grooves.

A test overview of the non-referenced DCPD crack growth response of CT223 and CT224 is provided in Figure 49. The non-referenced DCPD response is used here because the resistivity evolution monitored by referenced DCPD is very close to zero, and the crack length noise level is reduced when using the non-referenced DCPD crack length. The test plan is to evaluate the SCCGR of both specimens in all the water chemistries specified in Table 1 through on-the-fly changes. As of this writing, the assessment of SCCGR of Alloy X-750 in BOC water chemistry containing Li vs. K has been completed. The test is currently evaluating the crack growth behavior of the two specimens in LiOH EOC water chemistry with 10 ppm B and 0.23 ppm Li.

The two specimens were loaded in series into an NRC SCC test system, and the test was started in the baseline PWR primary water condition containing 1500 ppm B and 2.2 ppm Li at 360 °C and 25 cc/kg H_2. Figure 50 presents the initial aggressive cycling in high-temperature water to further extend the precrack produced by air fatigue. A series of loading conditions were used to transition from the TG precrack to an IGSCC crack front that is typically much more susceptible to SCC growth in Ni-base alloys. Loading conditions started with cyclic loading with decreasing frequency from 1.0 to 0.01 Hz at a load ratio of 0.5, followed by a final cycling step of a 980 s rise and a 20 s fall (0.001 Hz) with R = 0.5 in a sawtooth form. The two specimens exhibited consistent crack growth behavior during these loading

steps, and the CGR continued to drop as the cyclic loading conditions became more and more gentle. However, after a hold time of 2.5 h was added at K_{max} (20 MPa√m in this case) to the 980s/20s cycling, the CGR unexpectedly increased by ~2X in both specimens (compare the 980s/20s corrosion fatigue CGRs in Figure 51 to the 980s/20s+2.5 hr hold corrosion fatigue CGRs in Figure 51). This has never been seen in testing of Alloy 600/690 and their weld metals at PNNL, but it has been observed by at least one other lab that has tested Alloy X-750 SCC growth behavior [10] and might be a unique trait of this precipitation-hardened high strength Ni-base alloy. The CGRs of the two specimens only dropped by a small fraction after constant K of 20 MPa√m was implemented, indicating a high susceptibility to SCC growth of this material in the baseline environmental condition. The observed constant K SCCGR values of ~5×10^{-7} mm/s at 360°C were considered too high for this test because the rapid crack growth would result in substantial crack extension before water chemistry changes could stabilize, leading to excessive crack extension that would cause the specimens to run out of usable crack extension before all planned assessments are completed. As a result, it was decided to drop the test temperature from 360°C to 325°C and increase the dissolved hydrogen content from 26 to 29 cc/kg. These changes would decrease the kinetics of SCC and bring the dissolved hydrogen level from the Ni/NiO stability line at 360°C to Ni-stable regime at 325°C, further reducing the SCC susceptibility of the material. As shown in Figure 51, the SCCGR of CT223 and CT224 dropped instantly from ~5×10^{-7} mm/s to ~$8–9\times10^{-8}$ mm/s after these changes were made. The new SCCGRs values were more manageable for the test, so it was decided to perform subsequent SCCGR assessments in this condition. This condition is closer to the actual environmental condition in plant and has been widely used as a prototypic simulated PWR primary water environment for SCC testing of susceptible materials.

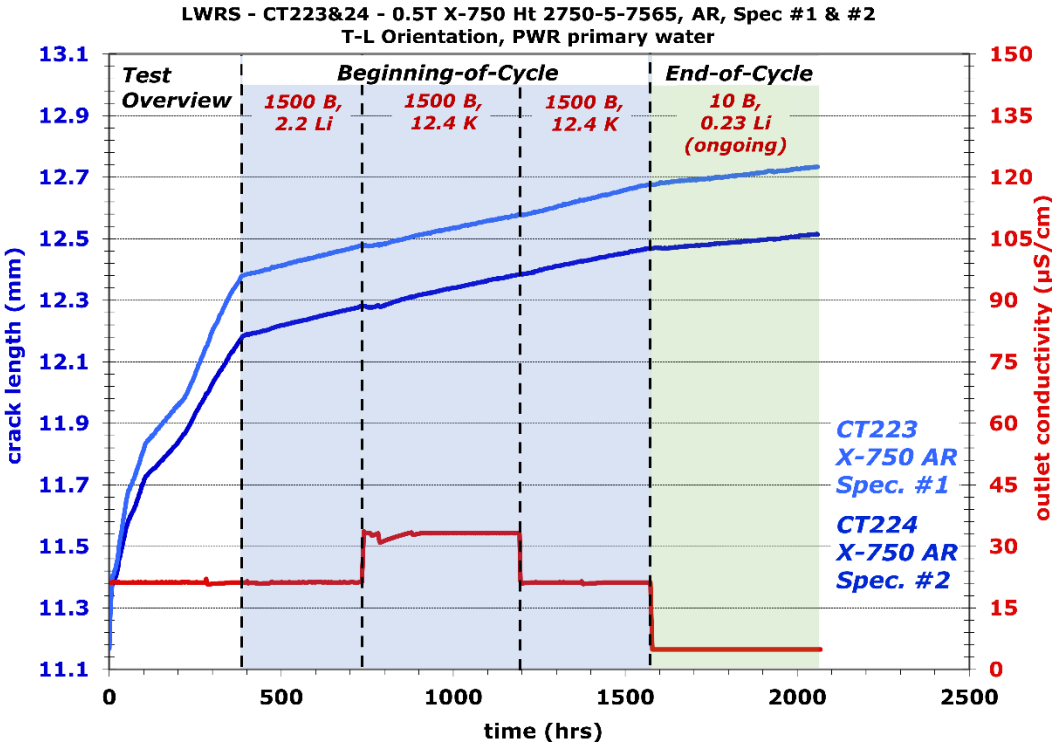

Figure 49. Test overview of crack growth response in the two Alloy X-750 specimens CT223 & 224 tested in T-L orientation. The effect of KOH vs. LiOH on the SCCGR of both specimens is being evaluated in 325°C simulated PWR primary water at a constant load of 20 MPa√m. The test is ongoing as of September 2021.

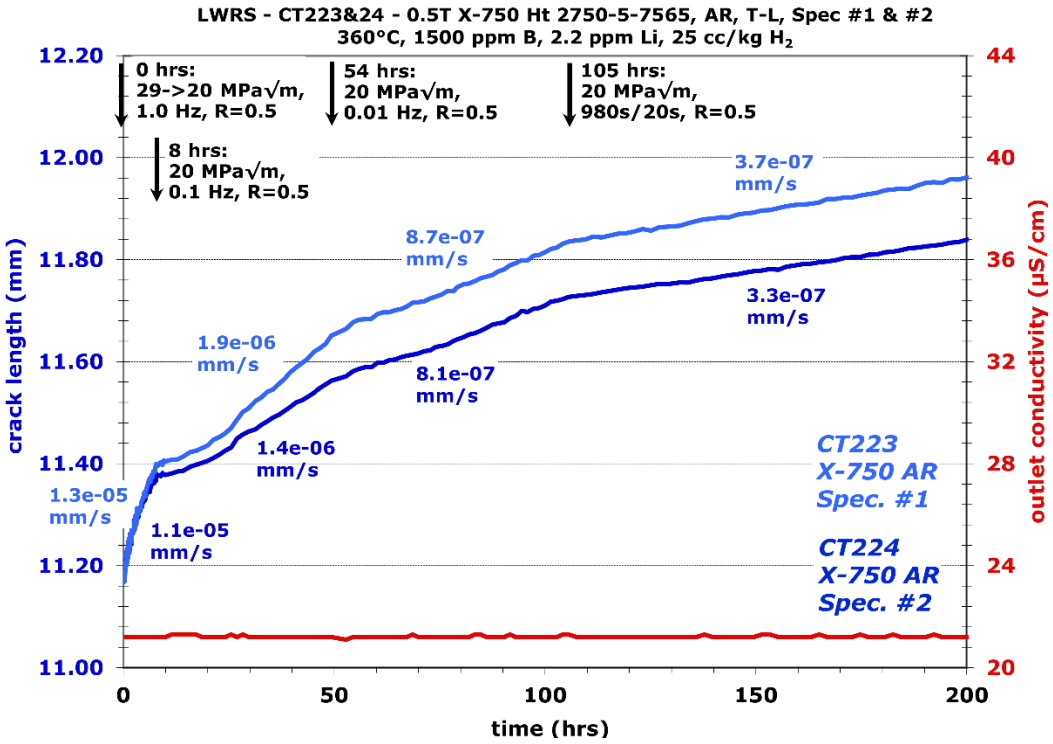

Figure 50. Crack growth response of the two Alloy X-750 specimens CT223 & 224 during initial cyclic loading transition steps in 360°C simulated PWR primary water.

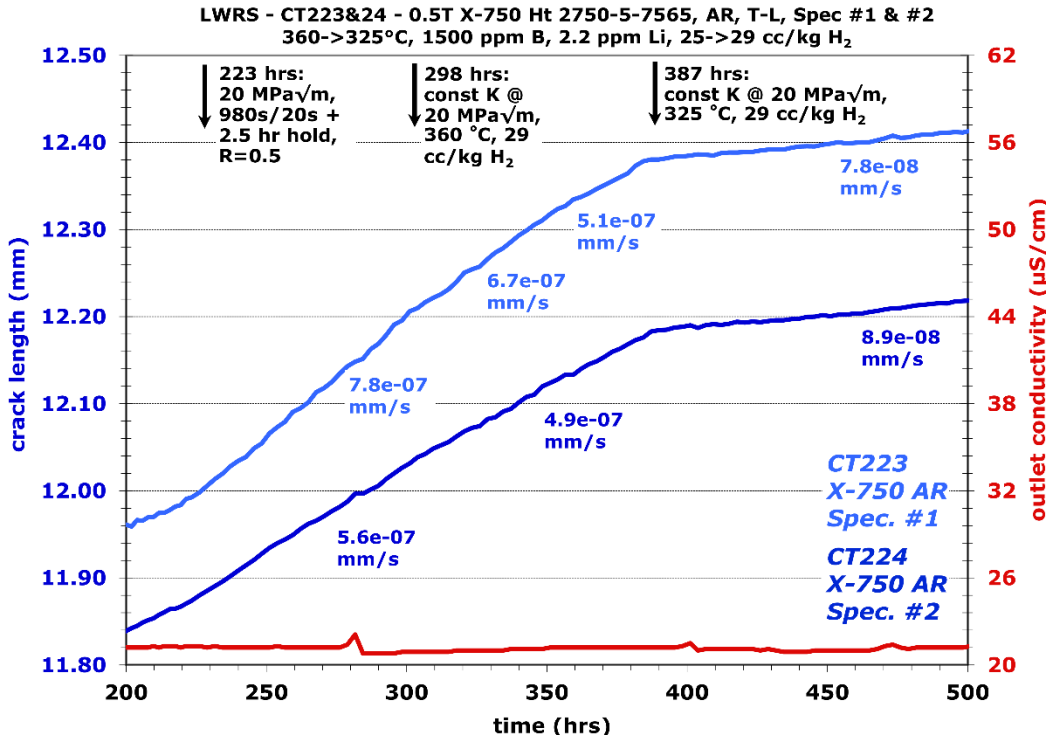

Figure 51. Crack growth response of the initial cycle+hold and constant load evaluation at 20 MPa√m of the two Alloy X-750 specimens CT223 & 224 in 360°C simulated PWR primary water with 25 cc/kg H_2. The water chemistry was then changed to 325°C and 29 cc/kg H_2 due to high SCCGR observed at 360°C and 25 cc/kg H_2.

4.3.1 SCC Growth Behavior in Beginning-of-Cycle Water Chemistry

The SCCGR evaluation of the effect of KOH vs. LiOH began with the BOC water chemistry at 325°C, 29 cc/kg H_2, and a constant load of 20 MPa√m. An overview of the SCCGR response of CT223 and 224 during the BOC evaluation period is provided in Figure 52. The ideal increment of crack length over which to measure a steady SCCGR is several grain diameters. However, since the Alloy X-750 material exhibits a bi-modal distribution in grain size distribution, determining an optimal crack extension to be evaluated for steady crack growth response is not straightforward. Figure 15 suggests that while the larger grains in the T-L plane are often >200 μm in size, a high density of clusters of much smaller grains are dispersed in the microstructure. Since the crack front in the CT specimens spans a total length of ~12 mm, multiple fine-grained clusters should be encountered at any given time as the crack grows. Therefore, we chose 100 μm as the preferred crack extension to observe SCCGR during each water chemistry evaluation. As shown in Figure 52, the evaluation started with 1500 ppm B/2.2 ppm Li, moved on to 1500 ppm B/12.4 ppm K after the crack extension reached ~100 μm in both specimens, and then back to 1500 ppm B/2.2 ppm Li to confirm behavior. All the water chemistry changes were performed on-the-fly following the procedure described in Section 2.2.4. The two specimens exhibited very consistent crack growth behavior throughout this entire evaluation, with a maximum change of ~17% in SCCGR between adjacent test steps, which is well within the uncertainty of the measurement method (Section 2.2.3). Therefore, it can be concluded that KOH BOC water chemistry does not affect the SCC growth behavior of Alloy X-750.

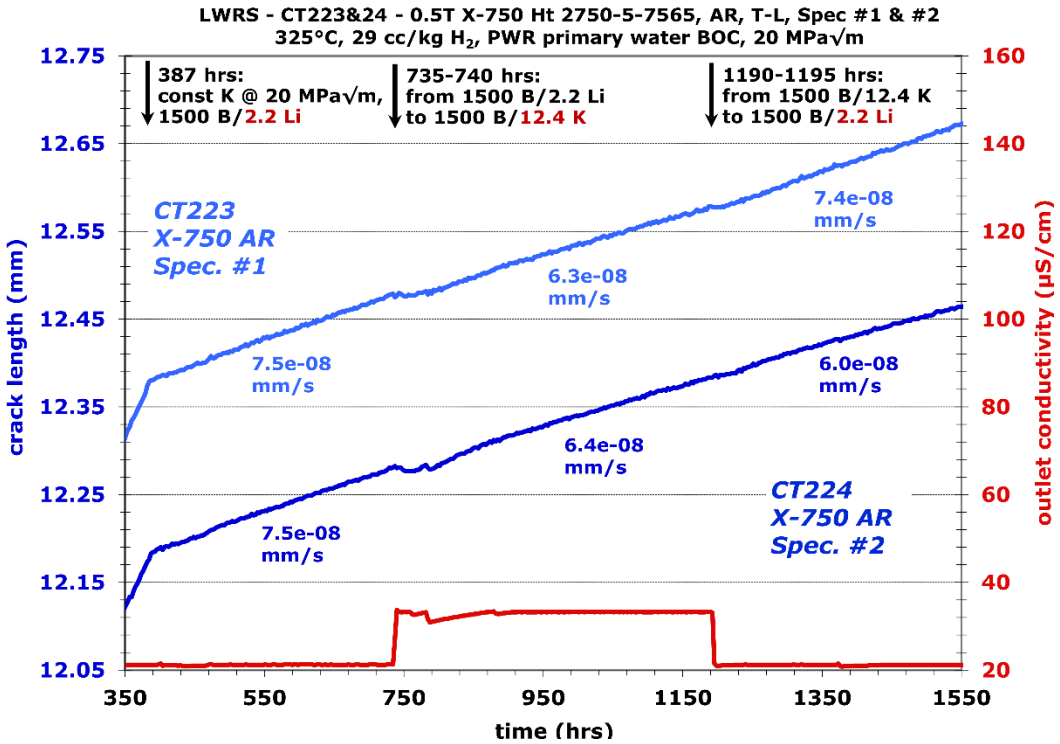

Figure 52. SCCGR response of the two Alloy X-750 specimens CT223 & 224 in 325°C PWR primary water BOC chemistry with on-the-fly changes between Li and K. The concentrations of B, Li, and K in the plot are shown in ppm.

4.3.2 SCC Growth Behavior in End-of-Cycle Water Chemistry

Once the SCCGR evaluation in the BOC water chemistry was completed, the test moved on to assess the effect of KOH vs. LiOH in the EOC water chemistry. An on-the-fly change from 1500 ppm B/2.2 ppm Li to 10 ppm B/0.23 ppm Li was implemented while all the other testing conditions were maintained the same. An obvious drop in SCCGR was observed in both specimens right after the change was made (Figure 53). The variation in SCCGR between the 10 ppm B/0.23 ppm Li EOC chemistry and the 1500 ppm B/2.2 ppm Li BOC chemistry in both specimens reached ~55–58%, suggesting a real decrease in SCCGR beyond the uncertainty of the measurement method. This was unexpected because most studies to date suggest no change in SCCGR in Ni-base alloys between low and high B/Li concentrations [23, 24]. A recent KOH vs. LiOH study on cold-worked Alloy 600 also showed that there was no change in SCCGR on shifting from the 1500 ppm B BOC chemistry vs. the 10 ppm B EOC chemistry [3]. Therefore, we decided to have CT223 and 224 expose for a longer duration in the current condition while closely monitoring their SCCGR response before determining the next step. As shown in Figure 53, as of this writing, the two specimens have been exposed in 10 ppm B/0.23 ppm Li EOC chemistry for ~500 hours, and the test is ongoing. Both specimens exhibit a similar and steady SCCGR at ~2.5–3.3×10^{-8} mm/s that remains clearly lower than the SCCGR observed in the 1500 ppm B/2.2 ppm Li BOC chemistry. As needed, additional testing steps will be applied to verify the true response in LiOH EOC conditions before switching to KOH EOC conditions.

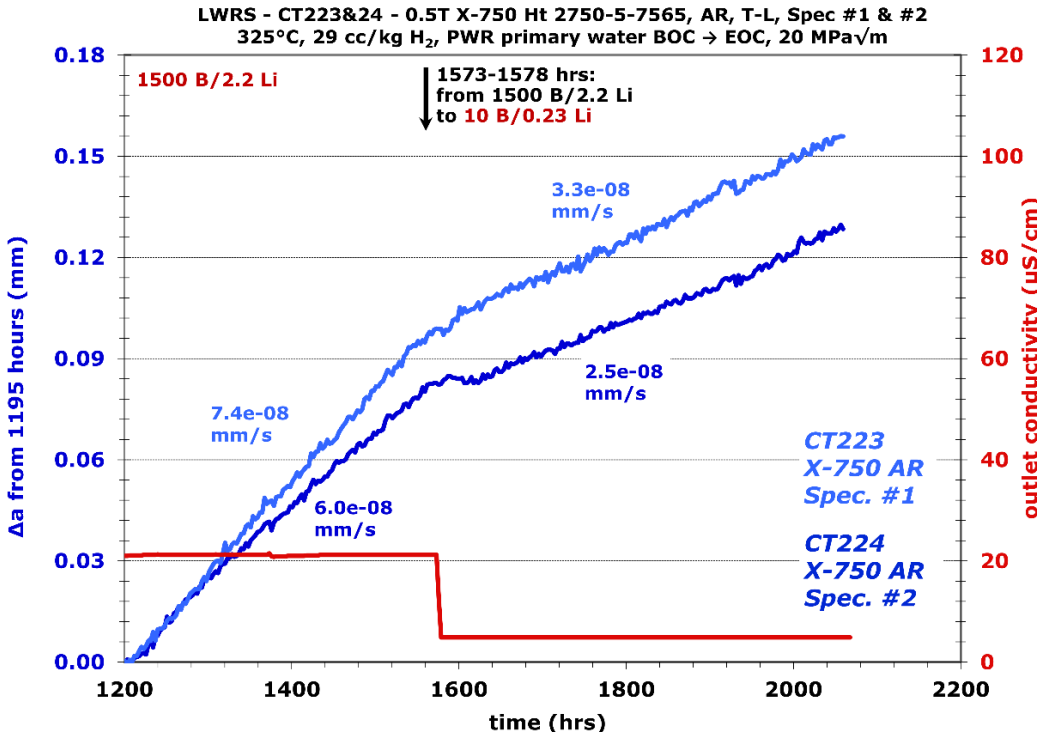

Figure 53. SCCGR response of the two Alloy X-750 specimens CT223 & 224 in 325°C PWR primary water with on-the-fly change from LiOH BOC to LiOH EOC water chemistry. The concentrations of B, Li, and K in the plot are shown in ppm. The test is currently evaluating the SCCGR of both specimens in EOC water containing 10 ppm B and 0.23 ppm Li (ongoing).

5. SCC CRACK GROWTH BEHAVIOR OF Alloy 718 IN KOH VS. LIOH-CONTAINING PWR PRIMARY WATER

Because Alloy 718PH has a reputation of being very resistant to PWSCC initiation but relatively susceptible to propagation once an IG crack is initiated, only SCC growth rate testing is carried out for this material to investigate the KOH vs. LiOH effect on SCCGR. In this chapter, the test procedure will be described, and the test status to date will be summarized for this ongoing test.

Two 0.5T CT specimens were extracted from the precipitation-hardened Alloy 718 block in the S-L orientation relative to the plate fabrication direction. This orientation was selected for its potentially maximized SCC susceptibility so that the test can be completed in a reasonable time frame. These two specimens, CT226 and CT227, were first fatigue precracked individually in air at room temperature following the procedure described in Section 2.2.2. The side grooves of these two specimens were polished to a 1 μm finish, allowing the precrack morphology to be viewed and its length to be measured. The results are shown in Figures 54 and 55 for CT226 and 227, respectively. CT227 exhibited a more uniform precrack length on both sides (1.045 vs. 1.136 mm) than CT226 (1.048 vs. 1.448 mm) and was therefore selected as the leading specimen for the SCC growth rate test. This means that the load control during the test would be implemented based on the response of CT227, whereas CT226 acts as a redundant companion specimen to confirm whether material behavior is reproducible under similar material and loading conditions.

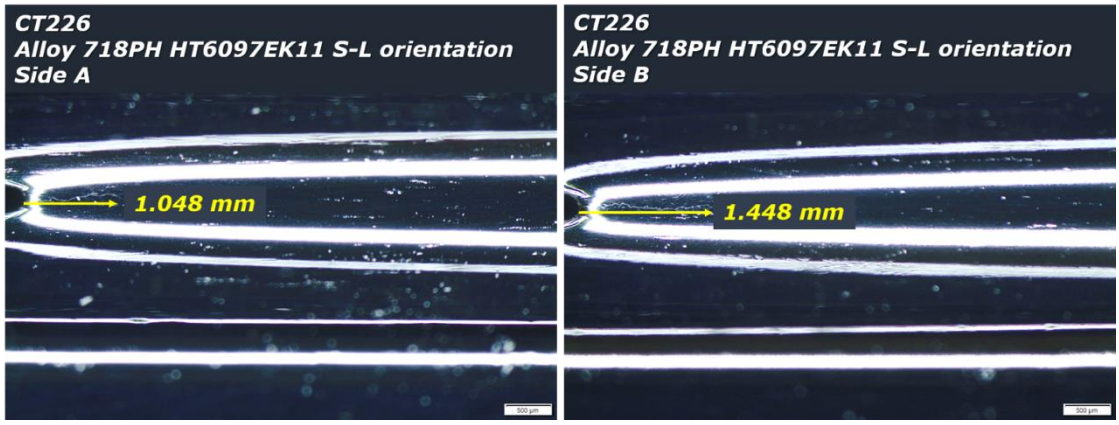

Figure 54. Optical micrographs of the polished side grooves of the Alloy 718PH specimen CT226. The length of the precrack produced by air fatigue is marked in both side grooves.

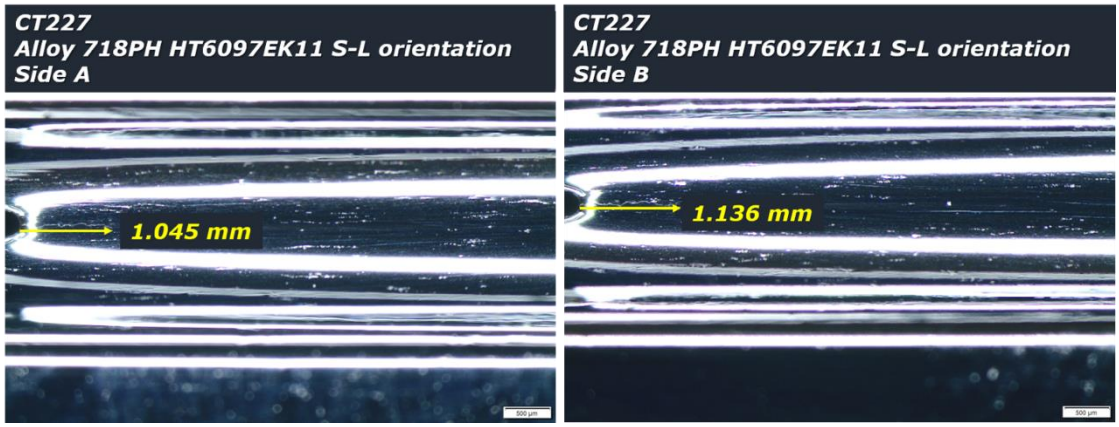

Figure 55. Optical micrographs of the polished side grooves of the Alloy 718PH specimen CT227. The length of the precrack produced by air fatigue is marked in both side grooves.

The two specimens were loaded in series into an NRC SCC test system, and the test was started in the baseline PWR primary water containing 1500 ppm B and 2.2 ppm Li at 360 °C and 25 cc/kg H_2. A test overview of the referenced DCPD crack growth response of CT226 and CT227 is provided in Figure 56. The test plan is to evaluate the SCCGR of both specimens in all the water chemistries specified in Table 1 through on-the-fly changes. As the writing of this report, the assessment of SCCGR of Alloy 718 has just begun in the first BOC water chemistry containing 1500 ppm B and 2.2 ppm Li. Figure 57 presents the initial cyclic loading steps implemented with decreasing frequency to transition the TG precrack produced by air fatigue to an IGSCC crack front. This includes cyclic loading from 1.0 to 0.01 Hz at a load ratio of 0.5 and a K_{max} of 20 MPa√m, followed by a final cycling step of a 980 s rise and a 20 s fall (0.001 Hz) with R = 0.5 in a sawtooth form. Decreasing CGRs were observed for both specimens during the more and more gentle cycling at each step. No further reduction in CGR was observed once a 2.5 h hold time was added to the final cyclic loading step (Figure 58), but this is not uncommon for materials that are highly susceptible to SCC growth. The absolute values of the SCCGR under these conditions was not as high as we had hoped, so to accelerate the test process, an increase in K_{max} from 20 to 25 MPa√m via dK/da was implemented over a crack extension of 15 μm, as can be seen in Figure 58. This produced an approximate 3x increase in CGR during cycle+hold loading which was deemed a sufficient increase in CGR to likely allow constant load observations to take place in a reasonable period of time. The test was then transitioned to constant load at 25 MPa√m. As of this writing, the two specimens have been evaluated for ~40 hours in the 1500 ppm B/2.2 ppm Li BOC water chemistry with similar initial SCCGRs at 1.2–1.3×10^{-7} mm/s. Since this Alloy 718PH material exhibits a consistent grain size of ~60 μm, the current plan is to observe the SCCGR in CT226 and 227 for a crack extension of 100 μm, after which an on-the-fly change from 1500 ppm B/2.2 ppm Li to 1500 ppm/12.4 ppm K will be made for uninterrupted SCCGR evaluation. The outcome of this test will be provided in a future report.

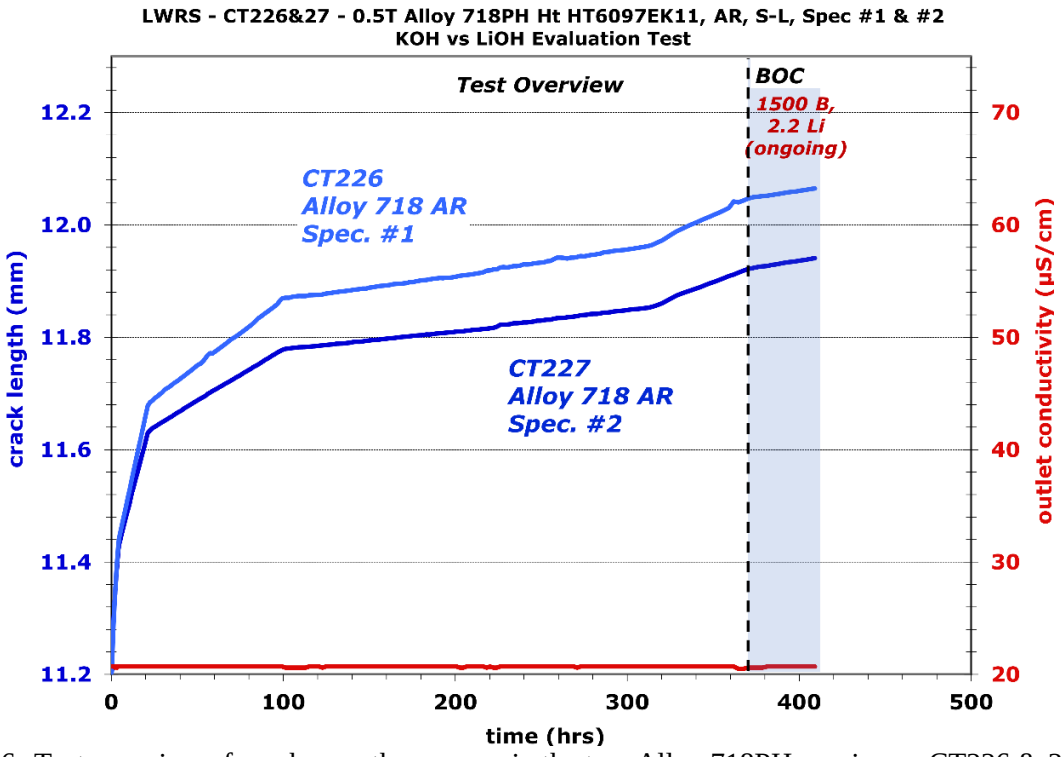

Figure 56. Test overview of crack growth response in the two Alloy 718PH specimens CT226 & 227 tested in S-L orientation. The effect of KOH vs. LiOH on the SCCGR of both specimens is being evaluated in 360°C simulated PWR primary water at 25 cc/kg H_2. The test is ongoing as of September 2021.

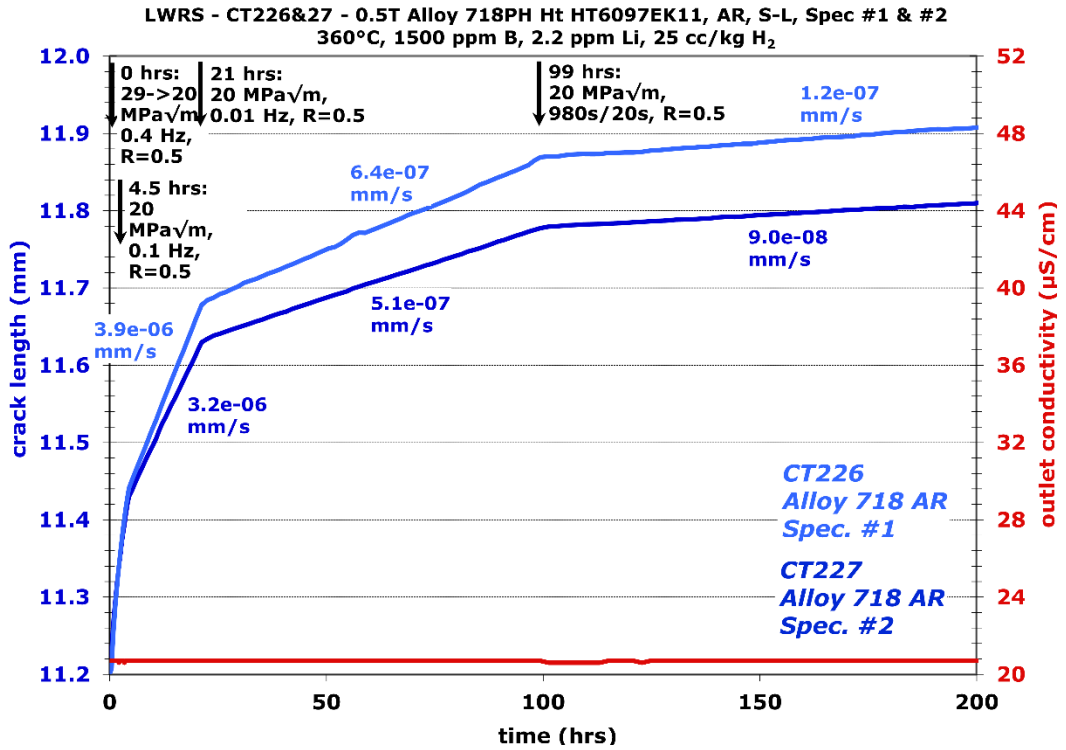

Figure 57. Crack growth response of the two Alloy 718PH specimens CT226 & 227 during initial cyclic loading transition steps in 360°C simulated PWR primary water.

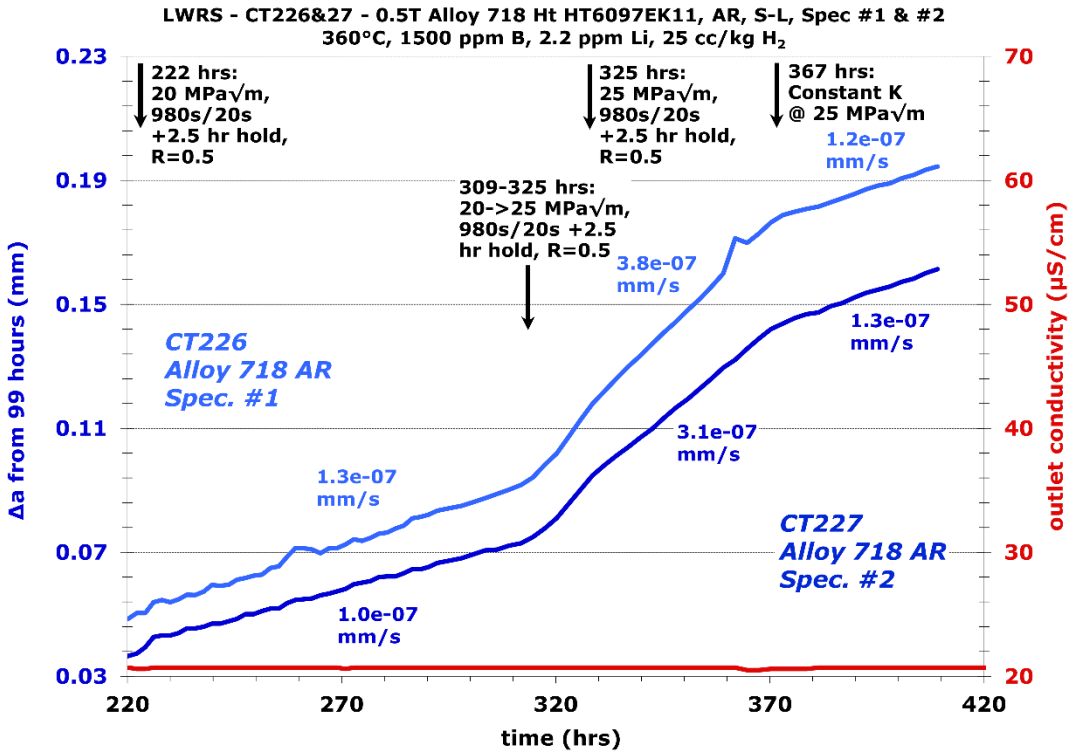

Figure 58. Crack growth response of the initial cycle+hold and constant load evaluation of the two Alloy 718PH specimens CT226 & 227 in 360°C simulated PWR primary water with 25 cc/kg H_2.

6. SUMMARY

The cost and availability of Li-7 is creating interest in using KOH to replace LiOH for primary system pH control in PWRs. A key concern regarding the use of KOH is its potential effect on the structural materials employed in the reactor internals, especially on Ni-base alloys where there is limited prior experience with exposure to KOH water chemistry. In collaboration with an ongoing EPRI-led qualification program to determine if KOH PWR water chemistry is acceptable from a materials degradation perspective as compared to LiOH PWR water chemistry, PNNL is performing supporting tests under LWRS to investigate whether replacing LiOH with KOH has a negative impact on the SCC behavior of Ni-base alloys. The testing materials and water chemistries were determined together with EPRI. In FY21, this study focuses on the high-strength Ni-base Alloy X-750 and Alloy 718.

For Alloy X-750, SCC initiation behavior in KOH BOC vs. LiOH water chemistries has been evaluated. The SCC initiation testing was performed in two test systems equipped with a DCPD technique for in-situ detection of SCC initiation. Two sets of six specimens were evaluated in 360°C PWR primary water BOC chemistry containing 1500 ppm B and either 2.2 ppm Li or 12.4 ppm K (i.e., molar-equivalent concentrations of KOH or LiOH to achieve neutral pH at 310°C). All specimens were tested at the material yield strength. While some scatter exists, the SCC initiation times of the specimens tested in these two water chemistries generally fall within the same range. Standard and censored Weibull analyses on the two data sets also revealed a large overlap in the 95% confidence intervals for any given cumulative failure probability. If anything, the SCC initiation time of Alloy X-750 in the KOH BOC water chemistry might be slightly longer than in the LiOH BOC water chemistry. In addition, post-test characterization found no obvious difference in the initiation morphology between these two sets of specimens. These results suggest that replacing LiOH with KOH would not adversely impact the SCC initiation susceptibility of Alloy X-750 in PWR primary water.

Meanwhile, SCC growth behavior is being evaluated on two Alloy X-750 CT specimens in the T-L orientation using in-situ measurement of crack extension by a highly refined DCPD method. The SCCGR evaluation of the effect of KOH vs. LiOH is underway at 325°C, 29 cc/kg H_2, and a constant load of 20 MPa√m. The water chemistries were changed on-the-fly, allowing uninterrupted, direct comparison of SCCGR in KOH vs. LiOH water chemistries with minimum disturbance to the test. As of September 2021, the SCCGR evaluation in the BOC water chemistry on KOH vs. LiOH has been completed and revealed no consequential difference. The test is currently evaluating the SCCGR of both specimens in the EOC water chemistry containing 10 ppm B and 0.23 ppm Li.

KOH vs. LiOH effect is also being evaluated for SCC growth behavior of two Alloy 718 CT specimens in 360°C PWR primary water with 25 cc/kg H_2 at a constant load of 25 MPa√m. The test is currently acquiring SCCGR data in the first BOC water chemistry containing 1500 ppm B and 2.2 ppm Li. At this point, there is not enough data to make any conclusions regarding the effect of KOH vs. LiOH on SCC growth behavior for Alloy 718. The progress of the SCC growth rate tests on Alloys X-750 and 718 will be updated in future reports.

REFERENCES

[1] P. Chou, J. Smith, A. Demma, M. Burke, K. Fruzzetti, Potassium Hydroxide for PWR Primary Coolant pH Control: Materials Qualification Testing, in: 21st NPC International Conference on Water Chemistry in Nuclear Reactor Systems, 2018, pp.

[2] K. Fruzzetti, A. Demma, P. Chou, J. Smith, D. Hussey, K. Kim, C. Gregorich, M. Burke, Potassium Hydroxide for PWR Primary Coolant pH Control: Qualification Program, in: 21st NPC International Conference on Water Chemistry in Nuclear Reactor Systems, 2018, pp.

[3] P. Andresen, P. Chou, SCC initiation and growth in PWR primary water containing KOH vs. LioH, in: 19th International Conference on Environmental Degradation of Materials in Nuclear Power Systems - Water Reactors, American Nuclear Society, 2019, pp. 363-372.

[4] P.M. Scott, 2000 F.N. Speller Award Lecture: Stress Corrosion Cracking in Pressurized Water Reactors—Interpretation, Modeling, and Remedies, Corrosion (Houston), 56 (2000) 771-782.

[5] P.L. Andresen, I.P. Vasatis, F.P. Ford, Behavior of short cracks in stainless steel at 288°C, in: CORROSION 1990, NACE, 1990, pp.

[6] E. Richey, D.S. Morton, M.K. Schurman, SCC initiation testing of nickel-based alloys using in-situ monitored uniaxial tensile specimens, in: 12th International Conference on Environmental Degradation of Materials in Nuclear Power Systems - Water Reactors, The Minerals, Metals & Materials Society, 2005, pp. 947-956.

[7] Z. Zhai, M.B. Toloczko, M.J. Olszta, S.M. Bruemmer, Stress corrosion crack initiation of alloy 600 in PWR primary water, Corrosion Science, 123 (2017) 76-87.

[8] S.M. Bruemmer, M.J. Olszta, D.K. Schreiber, M.B. Toloczko, Stress Corrosion Crack Initiation of Cold-Worked Alloy 600 and Alloy 690 in PWR Primary Water, Pacific Northwest National Laboratory: Technical Milestone Report M2LW-14OR0404023, Light Water Reactor Sustainability Program, DOE Office of Nuclear Energy, September 2014.

[9] M.B. Toloczko, N.R. Overman, M.J. Olszta, S.M. Bruemmer, Pacific Northwest National Laboratory Investigation of Stress Corrosion Cracking in Nickel-Base Alloys, Volume 3: Stress Corrosion Cracking of Cold-Worked Alloy 690, NUREG/CR-7103 Vol. 3, Nuclear Regulatory Commission, Office of Nuclear Regulatory Research, 2015.

[10] P.L. Andresen, J. Flores-Preciado, M.M. Morra, R. Carter, Microstructure and SCC of Alloy X-750, in: 15th International Conference on Environmental Degradation of Materials in Nuclear Power Systems-Water Reactors, John Wiley and Sons Inc., 2011, pp. 679-700.

[11] J.H. Jackson, S.P. Teysseyre, Baseline Fracture Toughness and CGR Testing of Alloys Alloy X-750 and XM-19 (EPRI Phase I), INL/EXT-11-24173, February 2012.

[12] A.A. Stein, M.S. Gennaro, Material specification for Alloy X-750 for use in LWR internal components, EPRI Report NP-7032, 1990.

[13] C. Benhamou, J.L. Chambrin, P. Todeschini, J. Champredonde, E. Lemaire, Evolution de la conception, de la fabrication et du montage des broches de fixation des tubes guides de grappes en Alliage X750, in: Proceedings Convention Nationale SFEN, 2004, pp.

[14] M.M. Morra, BWRVIP-240: BWR Vessel and Internals Project, Metallurgical Analyses and Macro and Microstructural Mapping of Alloy X-750 and Alloy XM-19 Plates, EPRI Report 1021003, August 2010.

[15] Alloy 718 Review for Fuel Assembly Applications, EPRI, Palo Alto, CA: 2013. 3002002176., December 2013.

[16] M.T. Miglin, J.V. Monter, C.S. Wade, J.K. Tien, J.L. Nelson, Stress corrosion cracking of chemistry and heat treat variants of alloy 718. Part 1: Stress corrosion test results, in: 6th International Symposium on Environmental Degradation of Materials in Nuclear Power Systems - Water Reactors, The Minerals, Metals & Materials Society (TMS), 1993, pp. 815-819.

[17] M. Wang, M. Song, G.S. Was, J.L. Nelson, The roles of thermal mechanical treatment and δ phase in the stress corrosion cracking of alloy 718 in primary water, Corrosion Science, 160 (2019) 108168.

[18] S. International, AMS5596 - Nickel Alloy, Corrosion and Heat-Resistant, Sheet, Strip, Foil and Plate 52.5Ni-19Cr-3.0Mo-5.1Cb (Nb)-0.90Ti-0.50Al-18Fe Consumable Electrode Remelted or Vacuum Induction Melted 1775 °F (968 °C) Solution Heat Treated, in, 1964.

[19] S. International, AMS5663 - Nickel Alloy, Corrosion and Heat Resistant, Bars, Forgings, and Rings 52.5Ni-19Cr-3.0Mo-5.1Cb(Nb)-0.90Ti-0.50Al-19Fe, Consumable Electrode or Vacuum Induction Melted 1775°F (968°C) Solution and Precipitation Heat Treated, in, 1965.

[20] Z. Zhai, M.J. Olszta, M.B. Toloczko, Quantitative Analysis of Precursor Damage and Crack Evolution in Alloy 690 and Its Weld Metals after Long-Term SCC Initiation Testing in PWR Primary Water, Pacific Northwest National Laboratory: Technical Milestone Report M3LW-21OR0402033, Light Water Reactor Sustainability Program, DOE Office of Nuclear Energy, April 2021.

[21] Z. Zhai, M.B. Toloczko, S.M. Bruemmer, Stress Corrosion Crack Initiation Behavior of Alloy 600 and Alloy 690 in PWR Primary Water, Pacific Northwest National Laboratory: Technical Milestone Report M2LW-18OR0402034, Light Water Reactor Sustainability Program, DOE Office of Nuclear Energy, September 2018.

[22] M.B. Toloczko, Z. Zhai, J. Wang, M.J. Olszta, R.A. Bouffioux, Materials Reliability Program: Stress Corrosion Crack (SCC) Initiation Testing of Ni-Base Alloys for PWR Applications Part 2 (MRP-448), EPRI Report #3002018002, June 2021.

[23] P.L. Andresen, Materials Reliability Program: Effects of B/Li/pH on PWSCC Growth Rates in Ni-Base Alloys (MRP-217), EPRI, Palo Alto, CA: 2007. 1015008., 2007.

[24] P.L. Andresen, J. Hickling, K.S. Ahluwalia, J.A. Wilson, Effects of PWR primary water chemistry on PWSCC of Ni alloys, in: 13th International Conference on Environmental Degradation of Materials in Nuclear Power Systems - Water Reactors, Canadian Nuclear Society, 2007, pp. 1393-1413.